Cardiovascular Research Institute

Research Day 2024

June 7, 2024

Katz Lecture Theater & Atrium

UNIVERSITY OF ALBERTA

Contents

WELCOME

Director's Message

Welcome to Research Day 2024! Thank you for joining us.

Cardiovascular research continues to be an amazing area of strength here at the University of Alberta; we are leaders in our field and our research makes a difference. The Cardiovascular Research Institute is proud to support this notable research community and today's event is all about celebrating accomplishments and sharing the progress that has been made in this last year.

We have a busy and exciting day planned. We are pleased to welcome two excellent visiting speakers. Dr. Heather Ross from the University of Toronto will start off our day presenting as the Dvorkin Lecturer at Medical Grand Rounds with a very timely presentation about digital health in the cardiovascular realm. Dr. Peter van der Meer from the University Medical Center Groningen is our Keynote Speaker for the afternoon session and will walk us through some of the tools he has been studying to bridge the gap from bench to bedside. Both are sure to be engaging and informative. The remainder of the agenda is focused on our trainees. Trainees play critical roles in the research work of today and in becoming the innovative leaders of tomorrow who will continue the fight to eliminate the burden of cardiovascular disease in the future. Several of the exceptional abstracts submitted by our trainees have been chosen to be presented from the podium and the remaining, but no less important, abstracts will be presented as posters. Based on input from last year's participants, we have adapted today's schedule to allow for more time to spend more time perusing the posters, talking with the presenters and networking with your peers.

I want to take a moment to thank the University of Alberta Advancement team, the University Hospital Foundation, the Royal Alexandra Hospital Foundation and all of our industry sponsors for their generous support. Events like these are an important way to share our work, foster collaborations and inspire new ideas, but none of this can occur without financial help. I also want to thank our Organizing Committee, Drs. Christi Andrin, Debraj Das, Jason Dyck, Michelle Graham, Rod MacArthur, Sean McMurtry, Carla Prado and Ms. Lisa Soulard, for all the time they have invested to make this event happen.

We hope you enjoy the day.

Justin A. Ezekowitz, MBBCh, MSc
Professor of Medicine
Director, Cardiovascular Research, University of Alberta
Co-Director, CVC
Cardiologist, Mazankowski Alberta Heart Institute
AHS Chair in Cardiac Sciences
President, Canadian Heart Failure Society

ACKNOWLEDGEMENTS:

This event is made possible through the generous support of the University and Royal Alexandra Hospital Foundations, an Educational Grant from Novo Nordisk®, and the following sponsors*:

Gold Sponsorship

- Cytokinetics Inc.

Silver Sponsorship

- AstraZeneca Canada
- Bayer Canada
- Bristol-Myers Squibb Canada Co.
- Merck Canada
- Pfizer Canada Inc.

**NOTE: The data and opinions presented at CVRI Research Day 2024 do not necessarily reflect the views or opinions of any of the sponsors or supporters.*

AWARDS:

In addition to the supporters and sponsors listed above, the trainee awards presented today are generously supported through the following:

Research Day Presentation Awards:

- Royal Alexandra Hospital Foundation

Cardiology Awards:

- Henry Anton Deutsch Fund
- Jose Galante Chicurel Fund

VISITING SPEAKERS:

Medical Grand Rounds & Dr. Joseph Dvorkin Memorial Lecture

"Digital Health for Heart Failure"

presented by Dr. Heather Ross

Dr. Heather Ross CM, MD, DSc, MHSc, FRCP (C), FACC

Division Head, Cardiology
Peter Munk Cardiac Centre

Professor of Medicine
University of Toronto

Heather Ross CM, MD, DSc, MHSc, FRCP (C), FACC is a Professor of Medicine at the University of Toronto, and Head of the Division of Cardiology at the Peter Munk Cardiac Centre. She received the Order of Canada in 2020 (CM), and an Honorary Doctor of Science (DSc) from Queen's University 2021. She is the Scientific lead for the Ted Rogers Centre for Heart Research, and holds the Loretta A. Rogers Chair in Heart Function and the Pfizer Chair in Cardiovascular Research. She received her medical degree from the University of British Columbia, Canada, Cardiology training at Dalhousie University, and Postdoctoral Fellowship in Cardiac Transplantation at Stanford University, California. She earned her Master's Degree in Bioethics from the University of Toronto. She has published over 400 peer reviewed articles, with an H index of 73 and > 23kcitations, trained > 45 highly qualified personnel and received > 40 million dollars in peer reviewed research funding**.** She has won numerous awards including Inventor of the year (UHN 2022), the Canadian Society of Transplantation Lifetime Achievement Award (2022), the inaugural CCS Women in Cardiovascular Medicine/Science Mentorship Award (2020) and the Canadian Heart Failure Society Annual Achievement Award (2019).

Keynote Lecture

"Translational Tools to Improve Personalized Medicine in Cardiology"

Presented by Dr. Peter van der Meer

Professor Peter van der Meer, MD, PhD
Chair, Department of Experimental Cardiology, University Medical Center Groningen

Professor of Heart Failure and Translational Cardiology, University of Groningen

Dr. Peter van der Meer is a cardiologist and chair of the Department of Experimental Cardiology at University Medical Center Groningen. He is also a Professor of Heart Failure and Translational Cardiology at the University of Groningen. Professor van der Meer received both his MD and PhD cum laude from the University of Groningen, and completed a postdoctoral fellowship at Harvard Medical School, Boston, MA, USA to train his skills in stem cell biology. His research group consists of PhD students and post-docs with various backgrounds (biologists, medical doctors and biomedical-engineers) working on translational research topics to bridge the gap between bench and bedside. Professor van der Meer's research focusses on understanding the susceptibility to develop heart failure and on exploring novel treatment targets and therapies.

Event Schedule

07:00 – 07:55	Registration & Poster Set-Up/Coffee & Pastries
08:00 – 08:05	Welcome & Introductions
08:05 – 09:00 Lecture	Medical Grand Rounds & Dr. Joseph Dvorkin Memorial Presenter & Keynote Speaker **Dr. Heather Ross, University of Toronto** **"*Digital Health for Heart Failure*"**
09:00 – 09:15	Coffee Break
09:15 – 10:15	Podium Abstract Session #1: **Recovery of Function** **Co-Chairs: Drs. Peter Light and Heather Ross** Presenter 1: **Yasser Abuetabh** *"Semaglutide Causes Cardiac Atrophy in Lean and Obese Mice"* Presenter 2: **Noah Hatch** *"Safety and Efficacy of Inclisiran in a Real-World Canadian High-Risk Population"* Presenter 3: **Jiyuan Piao** *"A novel small molecule synthesized based on a snail hibernation model, induces hibernation in mouse fibroblasts and perfused hearts"* Presenter 4: **Qiuyu Sun** *"Increasing ketone supply to the heart does not exert functional benefits in mice with heart failure with preserved ejection fraction (HFpEF)"* Presenter 5: **Jennie Vu** "*Investigating elamipretide as a potential therapeutic for sepsis-induced cardiac dysfunction"*

10:15 – 11:00 Coffee Break and Poster Session

11:00 – 11:50 Podium Abstract Session 2: **Vascular Function**

Co-Chairs: Drs. Micha Dorsch and Lisa Hornberger

Presenter 1: **Suha Jarad**

"The Role of VSMC MMP14 in The Development of Atherosclerosis"

Presenter 2: **Ezra Ketema**

"SIRT2 Inhibition Decreases Glycolysis and Attenuates Hypertrophic Response in H9c2 Cardiomyocytes"

Presenter 3: **Sophie Sigfstead**

"Prevalence, Burden, and Manifestation of Atrial Fibrillation: A large-scale analysis of long-term cardiac monitoring exams"

Presenter 4: **Xiaoying Wu**

"Progression of Atherosclerotic Cardiovascular Disease in Young Women with and without Polycystic Ovary Syndrome"

11:50 – 13:15 Lunch Break and Posters Session

13:15 – 14:15 Keynote Lecture

Dr. Peter van der Meer, University Medical Center Groningen

"Translational Tools to Improve Personalized Medicine in Cardiology"

14:15 – 15:05

Podium Abstract Session #3: **Cardiac Function**

Co-Chairs: Drs. John Ussher and Donna Vine

Presenter 1: **Wesam Bassiouni Farag**

" MMP-2 inhibitors attenuate ER stress-mediated myocardial cell death during ischemia-reperfusion injury"

Presenter 2: **Diego Castaneda-Zaragoza**

"Platelet from patients with acute myocardial infarction have an increased ratio of eNOS-negative to eNOS-positive platelets compared to healthy volunteers"

Presenter 3: **Aanchel Gupta**

"Hyperkalemia-related heart failure therapy discontinuation and its association with adverse outcomes in patients with heart failure: a population-based study"

Presenter 4: **Matthieu Zolondek**

"Improved mitochondrial respiration in a murine model of heart failure through the modulation of ROMO1"

15:05 – 15:45 Coffee Break and Poster Session

15:45 – 16:30

3 Minute Thesis-style Presentations

Co-Chairs: Drs. Carla Prado and Peter van der Meer

Presenter 1: Aleksandra Franczak

"Dual role of angiostatin in COVID-19"

Presenter 2: Lynn Lunsonga

"The Sodium/Glucose Cotransporter 2 Inhibitor Empagliflozin Inhibits Long QT 3 Late Sodium Currents in a Mutation Specific Manner"

15:45 – 16:30	***3 Minute Thesis-style Presentations continued*** ***Co-Chairs: Drs. Carla Prado and Peter van der Meer***

Presenter 3: **Samar Nesr (Gerges)**

"Sex-dependent changes of cardiac cytochrome P450 enzymes and hydroxyeicosatetraenoic acids in pressure overload-induced cardiac hypertrophy in rats"

Presenter 4: **Andrea Shysh**

"New and persistent psychoactive medication use in intensive care survivors with COVID-19"

Presenter 5: **Saymon Tejay**

"Tumour Secreted Inosine and Hypoxanthine Promote RBFOX1 Degradation, Cardiomyocyte Dedifferentiation and Susceptibility to Cardiotoxicity"

Presenter 6: **Fulin Wang**

"Characterizing the left ventricular transcriptome of donation after circulatory death (DCD) porcine hearts undergoing prolonged ex situ heart perfusion (ESHP) in the absence and presence of a multi-drug postconditioning treatment"

Presenter 7: **Yongneng Zhang**

"A critical contribution of cardiac myofibroblasts and a predictive role of UCP2 SNPs in the RV decompensation in pulmonary hypertension"

16:30 – 16:45	Networking (Q&A with Speakers) and Poster Take-Down
16:45 – 17:00	Awards & Concluding Remarks
17:00	**Reception – Katz Atrium**

ABSTRACTS

All abstracts submitted in alphabetical order by submitter's last name

Session 1, Recovery of Function oral presentation

Semaglutide Causes Cardiac Atrophy in Lean and Obese Mice

Yasser Abuetabh, PhDa; Matthew D. Martens PhDa, Mya A. Schmidt, BSca, Matthieu Zolondek, BSca; Heidi L. Silvera, Jody L. Levasseura, and Jason R.B. Dyck, PhDa*.

BACKGROUND
The significant reduction in body weight (BW) induced by glucagon-like peptide-1 receptor agonists (GLP-1RAs), such as semaglutide, has led to recent clinical trials demonstrating benefit in certain forms of cardiovascular disease (CVD). While these findings are promising for CV patients, one side-effect of GLP-1RAs use is the loss of skeletal muscle (lean BW) mass. This loss of lean BW could lead to exercise intolerance that may reduce the quality of life in certain patient populations with CVD. Given this, intense research efforts are ongoing to try to understand how GLP-1RAs induce loss of skeletal muscle mass. However, little attention has been given to the potential that other types of muscle, such as cardiac muscle, may also be lost in response to GLP-1RAs.

METHODS/RESULTS
Obesity was induced in male mice by feeding a high fat, high sucrose diet for 10 weeks. The protocol causes BW gain in the absence of inducing cardiac structural or functional changes. Following this, mice were switched to a regular chow diet and administered 120 mg/kg/day semaglutide for 21 days. As expected, mice treated semaglutide lost ~30% of their BW and ~65% of their fat mass compared to vehicle-treated mice. No changes in systolic or diastolic function were observed in these 2 groups as assessed by echocardiography. However, semaglutide induced a significant reduction in echocardiographic assessed left ventricular (LV) mass (16.51% decrease, $p<0.0001$), overall heart weight (12.84% decrease, $p<0.0006$), and histologic assessed cardiomyocyte area (30.37% decrease, $p<0.0001$). There were no changes in atrophy or fibrosis gene transcripts. Lastly, lean mice treated as the obese mice displayed no changes in BW but did show similarly decreased LV mass, overall heart weight, and cardiomyocyte area, indicating that the reduction in cardiac size induced by semaglutide occurs independent of weight loss.

CONCLUSIONS
Overall, these data show that semaglutide has a direct effect on the cardiomyocyte and induces a reduction in cardiac mass and suggest that like skeletal muscle, the same effect may be observed in hearts of individuals taking semaglutide. This information is extremely important given the growing trend of administrating GLP-1RAs to CV patients and the potential to alter cardiac structure in settings that may be adversely impacted by reduced cardiac mass. Thus, we suggest that until clinical studies have fully characterized the cardiac effects of GLP-1RAs, careful monitoring of cardiac structure in CV patients may be warranted.

Poster #1

Robotic-Arm Assisted Multiple Apical-View 3D Fusion of Echocardiography for Enhanced Right Ventricular Assessment and Measurement.

Khalid Alquwaynim , Kumaradevan Punithakumar and Michelle Noga

BACKGROUND
Historically, the RV has received less attention than the left ventricle (LV) in cardiac research despite its critical impact on cardiovascular disease outcomes. The RV's complex anatomy presents unique challenges for echocardiographic evaluation, often resulting in suboptimal image quality and diagnostic accuracy. Traditional three-dimensional echocardiography (3DE) struggles with issues such as limited field of view (FOV) and poor SNR, which hinder comprehensive assessment. Multi-view 3-D echocardiography (M3DFE) has emerged as a solution by fusing multiple 3DE datasets from various acoustic windows, yet precise spatial alignment remains a challenge (1). This study explores the integration of a robotic arm to enhance 3DE by providing accurate 3D transducer tracking, aiming to fuse different apical views from different windows more effectively and improve RV assessment quality. The proposed approach, believed to be the first of its kind, tests the hypothesis that robotic-assisted data fusion can lead to superior RV function and structure evaluations, tested on both volunteers and a select patient group.

METHODS/RESULTS
Enrolment: Utilized datasets from the Mazankowski Alberta Heart Institute include 20 echocardiographic scans—15 from healthy volunteers and five from patients—approved by the University of Alberta's Health Research Ethics Board. System component and scanning protocol: Precision in image acquisition was achieved using the UR10e robotic arm paired with a Philips EPIQ 7C ultrasound scanner for volunteer scans (2). The protocol incorporated multi-beat acquisition across apical and parasternal 3D views to construct detailed cardiac sub-volumes. We employed the same protocol for patient scans but without the robotic arm. Image processing: Echocardiographic data, initially in Cartesian form, were converted to NRRD using 3D Slicer, ensuring essential spatial and temporal alignment for accurate single-view fusion. Subsequent fusion employed averaging (via a Python script) and wavelet-based methods (via 3DSlicer module).
Image Analysis: Quantitative assessment involved SNR and CNR calculations for both fused and non-fused images. RV volume measurements were analyzed using TomTec for non-fused images and 3DSlicer for fused images, with cross-validation for reliability. An ongoing user study is set to evaluate the fusion's effectiveness qualitatively.

CONCLUSIONS
The results reveal significant enhancement in image quality, with an increased SNR and CNR following fusion via wavelet and averaging techniques for RV. Data derived from the robotic arm (RA) echocardiography exhibited greater enhancements in SNR and CNR than those obtained manually (RE), underscoring the precision and repeatability afforded by the robotic arm technology. As we continue with the RV assessment analyses and the user study, we expect that the observed enhancements will lead to more precise evaluation in cardiac imaging. In conclusion, these findings highlight the robust potential of incorporating robotic assistance and fusion methods in echocardiography to achieve superior image clarity and detail, promising to refine cardiac diagnostics and patient care.

Table 1 Comparative SNR and CNR for Robotic Arm and Manual Echo Before and After Fusion.

Variables	3DE (n=20)		S3DFE WAV (n=20)		S3DFE AVG (n=20)	
	RA (n=15)	RE (n=5)	RA (n=15)	RE (n=5)	RA (n=15)	RE (n=5)
SNR	11.02 ± 12.52	7.64 ± 7.69	12.99 ± 15.35	11.94 ± 7.91	14.54 ± 15.26	9.54 ± 7.80
CNR	4.99 ± 4.47	8.16 ± 6.53	8.98 ± 9.72	8.38 ± 7.37	5.88 ± 5.52	6.13 ± 5.62

Values are given as mean ± SD.

3DE= Three-Dimensional Echocardiography; S3DFE= Single-View Three-Dimensional Fusion Echocardiography SNR= Signal to Noise Ratio; CNR= Contrast to Noise Ratio; WAV= Wavelet Fusion; AVG= Averaging Fusion; RA= Robotic Arm; RE= Regular Echocardiography.

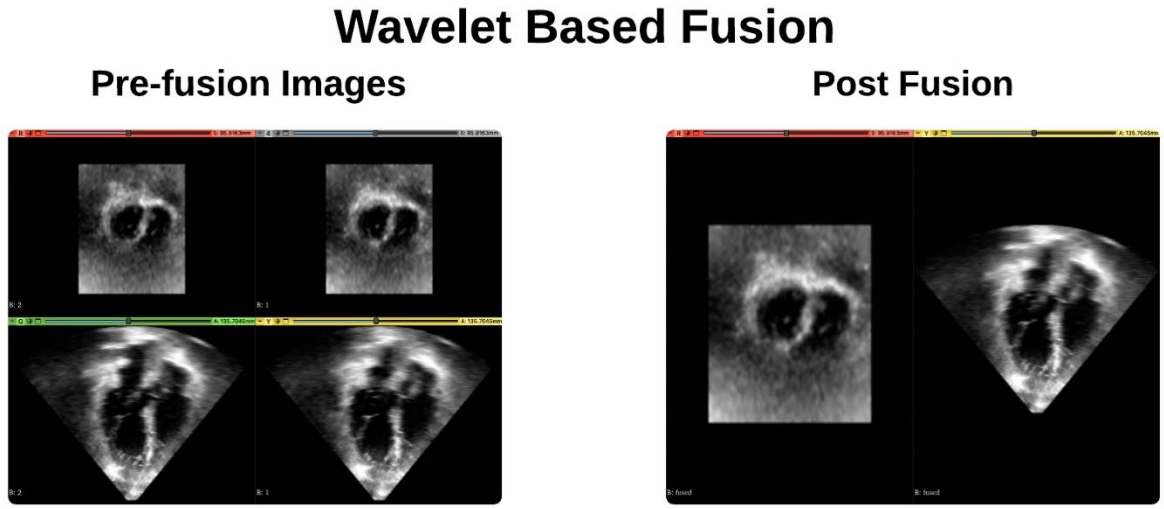

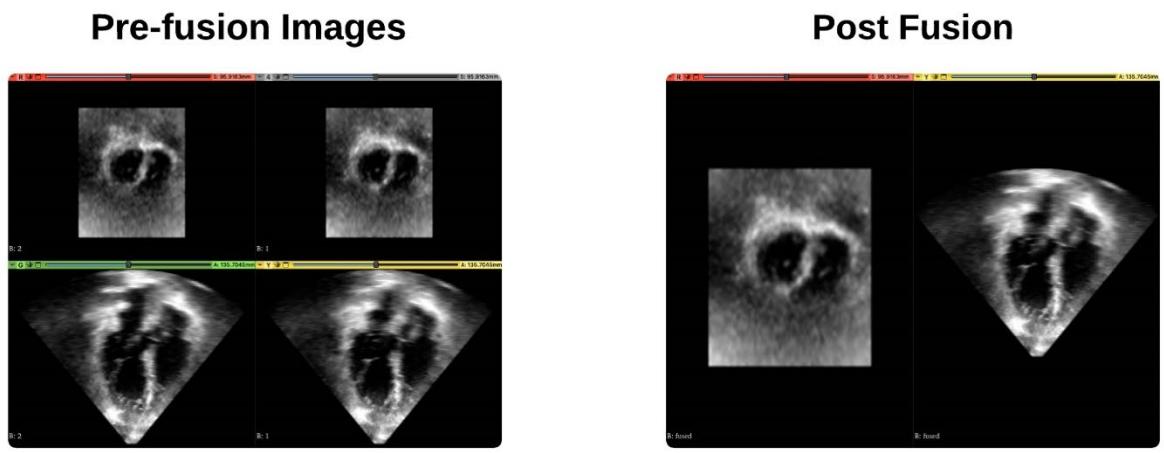

Poster #2

COVID-19 Promotes Generation of Pro-thrombotic eNOS-Negative Platelets: Potential Role of Inflammatory Response

Amir Asgari, Aleksandra Franczak, Alex Herchen, Glen Jickling, and Paul Jurasz1,2,4,5

BACKGROUND
Platelet-rich microvascular thrombi are common in severe COVID-19. Endogenous nitric oxide (NO)-signaling limits thrombus formation and previously we identified platelet subpopulations with a differential ability to produce NO based on the presence or absence of endothelial nitric oxide synthase (eNOS). eNOS expression is counter-regulated by cytokines, and recent reports demonstrate that COVID-19-associated immune/inflammatory responses affect the transcriptome profile of megakaryocytes and their platelet progeny. We investigated whether the ratio of eNOS-negative to –positive platelets increases in COVID-19 patients and whether this change may be due to the actions of pro-inflammatory cytokines on megakaryocytes.

METHODS/RESULTS
Methods: Platelets were isolated from hospitalized COVID-19 patients and COVID-19-negative controls. Platelet eNOS was measured by flow cytometry and plasma inflammatory cytokines by ELISA. Megakaryocytes from eNOS-GFP transgenic mice and the Meg-01 cell line were characterized to identify an appropriate model to study eNOS-based platelet subpopulation formation in response to inflammatory cytokines.
Results: COVID-19 patients demonstrated significantly elevated ratios of eNOS-negative to -positive platelets compared to controls and their ratios correlated with disease severity. Higher eNOS-negative to –positive platelet ratios were associated with enhanced platelet reactivity as measured by surface CD62P. Accordingly, amsalp 1-LI dna ,6-LI , -FNT rehgih detartsnomed stneitap 91-DIVOC concentrations than controls. Inflammatory cytokines associated with COVID-19 promoted eNOS-negative Meg-01 formation and enhanced subsequent eNOS-negative platelet-like particle formation.

CONCLUSIONS
COVID-19 patients have a high eNOS-negative to –positive platelet ratio, likely as a result of inflammatory response reducing megakaryocyte/blast eNOS expression, which predisposes them to thrombosis.

Session 3, Cardiac Function oral presentation

MMP-2 inhibitors attenuate ER stress-mediated myocardial cell death during ischemia-reperfusion injury

Wesam Bassiouni, Zabed Mahmud, Thomas Simmen, John M. Seubert, Richard Schulz

BACKGROUND
Matrix metalloproteinase-2 (MMP-2) is a ubiquitous protease that is activated intracellularly in response to oxidative stress during myocardial ischemia-reperfusion (IR) injury. Enhanced production of reactive oxygen-nitrogen species disrupts protein folding in the endoplasmic reticulum (ER) and induces ER stress. As a result, the unfolded protein response (UPR) is activated through different ER stress sensors including inositol-requiring enzyme 1α (IRE1α) and protein kinase R-like ER kinase (PERK), to restore protein folding. Failure of the UPR to reduce ER stress induces cellular dysfunction and apoptosis. MMP-2 localizes to the mitochondrial-ER-associated membrane. However, its role in ER homeostasis is unknown. We hypothesized that MMP-2 may proteolyze IRE1α during IR injury and stimulate ER stress-mediated myocardial cell death.

METHODS/RESULTS
Hearts from 3-month-old male mice subjected to in vitro IR injury (30 min global, no-flow ischemia followed by 40 min reperfusion) showed a significant reduction in left ventricular developed pressure compared to aerobically perfused controls. Ventricular extracts obtained from IR hearts at the end of reperfusion had higher levels of CHOP and caspase-3 and -9 activities in cytosolic fractions compared to aerobic controls, indicating induction of ER stress-mediated apoptosis in IR hearts. IRE1α and PERK levels were reduced in IR hearts compared to aerobic controls. MMP-2 preferring inhibitors, ARP-100 (10 μM) or ONO-4817 (50 μM), given 10 min before ischemia, improved post-ischemic recovery of left ventricular developed pressure compared to IR hearts (% of pre-ischemic baseline at end of reperfusion: IR+vehicle 27.2±7.3, IR+ARP 54.1±3.0, IR+ONO 64.8±5.3%, n=5 per group, $p<0.05$). Both ARP-100 and ONO-4817 attenuated the increase in CHOP and caspases activities and the reduction in IRE1α, but not PERK, compared to IR hearts ($p<0.05$). They also reduced infarct size and necrotic cell death in hearts subjected to a longer duration of 45 min ischemia and 120 min reperfusion. Incubation of mouse heart extract with exogenous MMP-2 showed evidence of IRE1α proteolysis.

CONCLUSIONS
During myocardial IR injury, MMP-2 activation may impair the UPR and induce myocardial cell death by proteolysis of IRE1α. Inhibition of MMP-2 activity protects against cardiac contractile dysfunction in part by preserving IRE1α and preventing ER stress-mediated cell death.

Poster #3

TRENDS IN PRIMARY FETAL CARDIOMYOPATHY: DIAGNOSES, OUTCOMES AND GENETIC ETIOLOGIES

Astha Burande, Lisa Hornberger, Oana Caluseriu, Jennifer Conway, Christy Cooke, Sue Chandra, Angela McBrien

BACKGROUND
Fetal cardiomyopathy (FCM) affects 8.24 per 100,000 live births, with 50%-82% neonatal mortality. Around 50% are idiopathic and 30% have extra-cardiac anomalies. The last decade has seen progress in fetal cardiac screening, genetic testing and management.

METHODS/RESULTS
Retrospective study conducted over a 5-year period (Jan 2017 - Dec 2021) of cases diagnosed with primary FCM in our program. The fetal database, echo reports, fetal and postnatal charts were reviewed.

Fifteen primary FCM were diagnosed at mean gestational age of 24+4 weeks. Subtypes were: 33% (5/15) non-compaction (NCM), 27% (4/15) restrictive (RCM), 20% (3/15) dilated (DCM), 13% (2/15) mixed (MCM), and 7% (1/15) left ventricular (LV) aneurysm. Extra-cardiac diagnoses: 33% (5/15) prenatally and 77%postnatally/ at postmortem (77% p=0.03). 87% (13/15) underwent genetic testing -60% (9/15) had likely/confirmed genetic etiology. Termination in 13% (2/15), intrauterine fetal death in 13% (2/15) and 73% (11/15) had live birth. At diagnosis, 14% (2/15) had hydrops, increasing to 40% (6/15) by delivery. 1-year survival was 55% (6/11): 100% (2/2) for MCM, 50% (2/4) for NCM, 50% (1/2) for RCM (25%), 50% (1/2) for DCM, and 0% (0/1) for LV aneurysm. 18% (2/11) used extracorporeal membrane oxygenation, 17% (3/11) had ventricular assist device and cardiac transplantation performed in 67% (2/3) of those listed.

CONCLUSIONS
Extra-cardiac diagnoses often accompany FCM, especially postnatally. Most FCM are associated with an identifiable confirmed/likely genetic etiology. Outcomes vary by subtype.

Session 3, Cardiac Function oral presentation

Platelet from patients with acute myocardial infarction have an increased ratio of eNOS-negative to eNOS-positive platelets compared to healthy volunteers.

Diego Castaneda-Zaragoza, Pishoy Gouda, Richard Schulz, Robert Welsh, Michelle Graham, Paul Jurasz

BACKGROUND
Incidence of and mortality from acute myocardial infarction (AMI) remains high despite current therapies. Previous studies have shown that nitric oxide (NO) produced by the endothelium is a potent inhibitor of platelet activation and aggregation. In addition to endothelial NO, platelets also are capable of producing NO which acts as a negative feedback mechanism limiting platelet activation and aggregation. Recently, our laboratory identified a platelet subpopulation that lacks the ability to produce NO due to the absence of the endothelial NO synthase (eNOS). This eNOS negative (eNOSneg) platelet subpopulation was shown to initiate adhesion and aggregation reactions, while eNOS-positive (eNOSpos) platelets limit aggregate size through their ability to generate NO. Further, we have shown that eNOSneg platelets may form from megakaryocytes(blasts) as a result of atherosclerosis-associated inflammation.
Therefore, we hypothesized that patients who have suffered an AMI have an increased ratio of eNOSneg to eNOSpos platelets compared to healthy controls, which might contribute to MI etiology.

METHODS/RESULTS
Blood samples were collected from 39 AMI patients (26 STEMI and 13 NSTEMI) and 8 healthy controls with a mean age of 65 years for controls, 62 years for STEMI and 59 years for NSTEMI (sex proportion of 37% males for controls, 61% for STEMI and 57% for NSTEMI). Platelets were isolated and eNOS-based platelet subpopulations were measured by flow cytometry. Additionally, platelet function studies were performed to assess platelet aggregatory response to collagen-coated sensors under flow conditions using a novel quartz crystal microbalance with dissipation (QCM-D) model.

Preliminary data demonstrated that platelets from AMI patients have an increased eNOSneg platelet subpopulation as a proportion of total platelets (26.1 ± 5.2%SEM for control, 61.3 ± 5.2% SEM for STEMI and 49.4 ± 5.6% SEM for NSTEMI, p=<0.05) (Figure 1). Furthermore, eNOSpos platelets from participants with AMI showed a lower mean fluorescence intensity compared to controls (2495 AU for controls vs. 1138 for STEMI vs. 1321 for NSTEMI), suggesting a lower amount of the eNOS enzyme in eNOSpos platelets.
Lastly, platelets from AMI participants showed a greater aggregatory response compared to healthy participants showing a greater negative change in frequency (-ΔF) when assessed using QCM-D (figure 2).

CONCLUSIONS
Platelets from AMI patients appear to have an increased eNOSneg/eNOSpos ratio compared to controls suggesting that a greater eNOSneg platelet subpopulation might contribute to the pathophysiology of AMI, consistent with previous reports of impaired platelet NO production in acute coronary syndromes. Further participant recruitment is on-going.

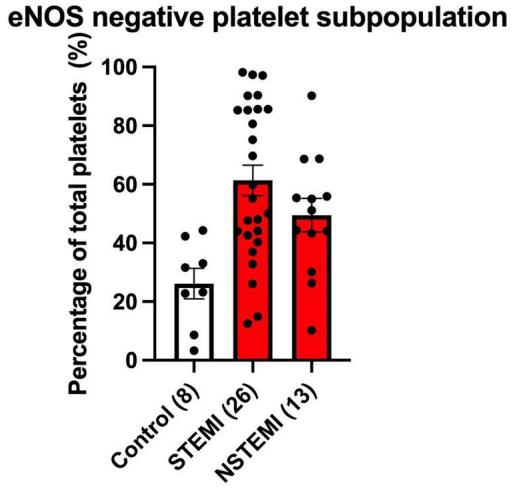

Figure 1.

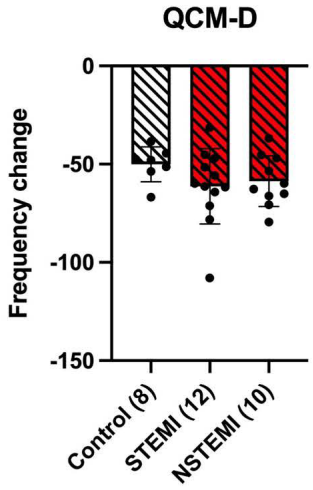

Figure 2.

Poster #4

A Hybrid Model for Automatic Segmentation of Colon Polyps in Colonoscopy Images Based on Adaptive Active Contours and Multi-scale Attention

Jingwen Cong

BACKGROUND
Early detection and segmentation of colon polyps using colonoscopy images are crucial for preventing colon cancer and enhancing early diagnosis, prognosis quality, and survival rates. In practical clinical settings, differences in imaging equipment and variations in the angles and intensity of lighting during capture can lead to significant changes in colonoscopy images. Moreover, the diversity of colon polyp types and their high variability in morphology, along with complex edge information, pose substantial challenges to existing computer vision segmentation methods.

METHODS/RESULTS
In this study, we introduce a novel automatic segmentation approach for colon polyp images that addresses the limitations of existing neural network-based methods and tackles the challenges arising from variations in colonoscopy images and the complex edge information inherent to polyps. Initially, we implemented a multiscale attention-based U-Net architecture as our backbone network. This architecture selectively concentrates on information across different scales in both spatial and channel dimensions, capturing more comprehensive hierarchical features. Furthermore, an adaptive active contour model equipped with self-adjusting evolutionary parameters has been integrated into the backbone network, allowing for dynamic adjustments of the evolutionary parameters in response to the characteristics of the input image.

CONCLUSIONS
Experimental results demonstrate that our proposed method achieves superior colon polyp segmentation performance across multiple datasets featuring diverse imaging conditions and polyp phenotypes.

Poster #5

Developing an Assay for Proteolyzed and Intact Cardiac Troponin I to Distinguish Patients Having Mild versus Severe Ischemic Disease

Kuldeep Dodia, Peter Hwang, Richard Schulz

BACKGROUND
Measurement of cardiac troponin in the blood is the most sensitive method to detect myocardial infarction. However, antibody-based troponin assays do not distinguish between patients presenting with a critical infarct or generalized cardiac strain. The unstructured regions of cardiac troponin I (cTnI) are susceptible to cleavage by proteases including matrix metalloproteinase-2 and calpains which are activated during infarction. Proteolysis of cTnI produces a heterogenous mixture of products in the blood that has confounded standardization. We suggest that reversible strain injury releases intact troponin, while necrotic cell injury from ischemia releases troponin fragments. We have previously shown that it is possible to differentiate intact troponin and its fragments using immunoassays that employ a combination of antibodies detecting different regions of cTnI. Our original immunoassays, however, did not have sufficient sensitivity for routine clinical use. Our aim is to develop a more sensitive and specific cardiac troponin assay which can distinguish between fragmented and intact troponin.

METHODS/RESULTS
An engineered soluble form of the cardiac troponin complex (eTn) was expressed in E.coli bacteria and purified for use as a reference material for the assay. Commercial antibodies targeting different epitopes of cTnI were conjugated to Acceptor and Donor AlphaLISA beads which release a quantifiable fluorescence signal upon close interaction. The major challenge is to find antibody pairs that bind the desired troponin species with high affinity and specificity. The linearity, reproducibility, and specificity of the assay will be assessed. A quantifiable signal was achieved using a combination of M18+625 and RecR85+560 antibodies and 2-fold dilutions of eTnI from 100 ng/mL to 0.78 ng/mL. The assay of serial diluted eTn concentrations with the candidate antibodies resulted in a linear curve in the ng/mL range. The optimized cTnI assay will be tested against human serum samples from a University of Alberta patient population displaying varying degrees of cardiac injury.

CONCLUSIONS
Further tests need to be conducted in the pg/mL range need to determine the limit of detection and reproducibility of the assay. The development of a more sensitive and specific cardiac troponin assay will provide a more accurate assessment of troponin in patients presenting with various mechanisms of cardiac injury.

Poster #6

Risk Factor Control in Patients with Documented Coronary Artery Disease in a large Metropolitan Cardiology Clinic

Dorsch EM, Tyrrell O, Suandork T, Das D, Cheung PK

BACKGROUND
Patients with coronary artery disease face heightened risk of recurrent events. Emphasizing risk factor control enhances long-term outcomes. Here, we assess risk factor control among coronary artery disease patients in a major metropolitan cardiology clinic.

METHODS/RESULTS
Six cardiologists from the same office participated. Using the electronic health record (Healthquest), we identified consecutive patients with diagnostic codes for ischemic heart disease or coronary artery disease billed from January 1, 2022, to July 31, 2022. Twenty patients per cardiologist were randomly selected. Patients were included if we could confirm previous acute coronary syndrome, revascularization, or at least 50% diameter stenosis on angiography or coronary CT angiogram. We documented guideline-recommended therapies (antiplatelets, lipid-lowering, ACE/ARB) and controlled modifiable coronary risk factors using available electronic health record data. Information was gathered hierarchically from lab results, doctor's letters, clinic notes, referral letters, patient questionnaires, and procedure reports. Smoking was deemed controlled if the patient wasn't currently smoking. Lipids were controlled if LDL was <1.8mmol/l, diabetes control required Hba1c <7%, and hypertension control necessitated systolic BP <130mmHg.

Fifty patients were excluded due to unconfirmed coronary artery disease diagnosis, replaced by randomly selected patients from the same cardiologist. Mean patient age was 67.0 (+/- 10.2) years, with 17.5% female representation. Initially, 64.2% presented with acute coronary syndrome. A high percentage were on antiplatelet/ antithrombotic (95.8%) and cholesterol-lowering agents (96.7%), while 76.7% were prescribed ACE/ARB drugs. Table 1 outlines modifiable risk factor control, and Figure 1 illustrates the percentage of patients with uncontrolled risk factors. Only 28.3% had all four risk factors managed.

CONCLUSIONS
We demonstrated strong adherence to guideline-recommended treatments, especially for cholesterol and antiplatelet therapies. However, documenting risk factors needs improvement. Concerningly, only 28% of patients with coronary artery disease have all risk factors controlled, despite specialist care. The crisis in family medicine might exacerbate this problem in the future. To tackle these gaps, we developed a structured, protocol-driven specialist clinic with allied healthcare professional assistance to enhance care quality. Clinic details and outcomes are in a separate abstract for this meeting (audit loop closure).

Table 1. Control of modifiable risk factors (n=120)

	Controlled (%)	Not controlled (%)	Unknown (%)
Smoking	70.8	9.2	20
LDL	49.2	34.2	16.6
Diabetes	62.5	19.2	18.3
Hypertension	43.3	47.5	9.2

Figure 1. (n=120)

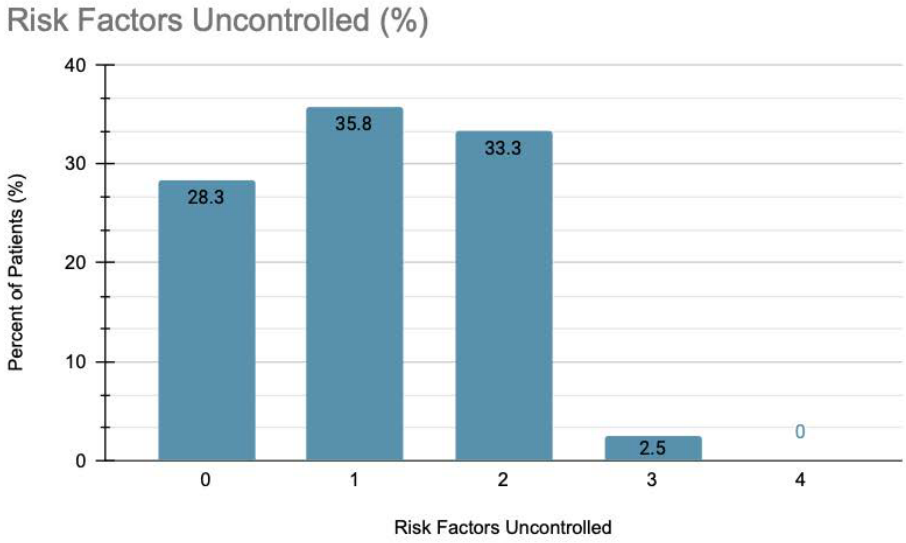

Session 4, 3MT-style presentation

Dual role of angiostatin in COVID-19

Aleksandra Franczak, Michael Joyce, Joaquin Lopez-Orozco, Tom C. Hobman, D. Lorne Tyrrell, Paul Jurasz

BACKGROUND
Angiostatin is a plasmin(ogen) break-down product constitutively generated by platelets in an urokinase(uPA)-dependent manner, and released during platelet thrombus formation. Microvascular thrombosis - a key pathological feature of severe COVID-19 – can create areas of high concentration of angiostatin and hypoxia, condition known to favour angiostatin's pro-apoptotic actions on endothelial and epithelial cells. The aim of the study was to assess role of angiostatin in COVID-19.

METHODS/RESULTS
Plasma samples from COVID-negative controls (n=17) and from hospitalized COVID-19 patients (n=30) were collected (day 1, 7, 14, 28) and compared between the groups. Second, to quantify angiostatin release by stimulated platelets, venous blood-isolated platelets (2.5x10^8/ml) with 1.5 microM plasminogen and with/without 30 microM aprotinin were activated with 3 microgram/ml collagen and incubated at 37°C for 4h, and platelet releasates were collected. Angiostatin was quantified via immunoblotting. Finally, mechanistic cellular studies investigated the effects of angiostatin and its neutralization on both SARS-CoV-2 infection and subsequent cell death. Cell death was assessed by percentage of cells detached from coverslips and/or TUNEL assay via fluorescence microscopy or flow cytometry. Immunofluorescent staining against the spike protein was used to confirm cellular infection.
Plasma angiostatin concentrations were significantly elevated in COVID-19 patients compared to COVID-19-negative controls at baseline (Mean±SEM: 28.1±3.9 vs 16.3 ±2.9 microgram/ml), and remained elevated for 21 to 28 days. Mean angiostatin concentration generated over 4h by activated platelets was 83.1±11.0 microgram/ml.
High angiostatin concentrations (140 microgram/ml) expected to be generated within a clot over 6-8 hours promoted death of VeroE6 cells and primary human bronchial epithelial cells (HBEC) in acidotic microenvironment (pH 6.9), as assessed during experiments where VeroE6 or HBEC were infected with SARS-CoV-2 and treated with angiostatin for 24h-48h. Irrespective of pH (pH 7.5 or 6.9), angiostatin reduced SARS-CoV-2 cellular entry of multiple SARS-CoV-2 variants, as assessed via flow cytometry of HEK-ACE2 cells infected with replication-incompetent GFP-expressing pseudo-viruses in the presence/absence of angiostatin (60-150 microgram/ml).
Selective angiostatin-neutralizing peptides inhibited angiostatin's cell death promoting effects but not its ability to reduce SARS-CoV-2 infection, as assessed with experiment where VeroE6 cells were infected with SARS-CoV-2 and treated with angiostatin in the presence/absence of selective angiostatin neutralizing or control peptides for 24h at pH 6.9.

CONCLUSIONS
Angiostatin has opposing roles in COVID-19 both preventing infection and promoting cell death. Selective angiostatin neutralizing peptides may be novel therapeutics for further pre-clinical evaluation in models of severe COVID-19.

Poster #7

Evaluating the burden of diabetes on heart failure related medical optimization and health status in a specialized clinic-based cohort

Luke Gagnon, Kaiming Wang, Chandu Sadasivan, Erik Youngson, Finlay A. McAlister, Gavin Oudit

BACKGROUND
Diabetes mellitus (DM) is a well-established risk factor for adverse prognosis in patients with heart failure (HF). We evaluated outcomes, quality of life (QoL) and guideline-directed medical therapy (GDMT) utilization in patients with DM and HF.

METHODS/RESULTS
Consecutive patients with HF attending appointments at the Mazankowski Alberta Heart Institure Heart Failure Clinic (HFC) were enrolled into a patient registry. 1,301 Patients were prospectively enrolled between February 2018 and August 2022. We examined all-cause mortality or deaths/cardiovascular hospitalizations in addition to QoL and GDMT utilization during this timeframe.

Patients with DM had higher rates of co-morbidities with the largest differences seen in hypertension (70.6% vs 43.8%), dyslipidemia (32.8% vs 16.9%) and chronic kidney disease (44.7% vs 26.1%), compared to those without DM (all p values < 0.001). Additionally, it was more common for patients with DM to have HF secondary to ischemic heart disease ($p < 0.001$). Patients without DM were more likely to have HFpEF compared to those with DM ($p < 0.05$, Figure 1A). The main significant difference in GDMT utilization was SGLT2i usage across all HF sub-types, which was much higher in the DM group (33.8% vs. 3.1%, $p < 0.001$, Figure 1B). In the heart failure with reduced ejection fraction (HFrEF) group for the overall cohort, GDMT utilization was 17.9% for SGLT2i, 96.5% for beta-blocker, 82.0% for MRA, and 94.6% for ACEi/ARB/ARNI (Figure 1B). Additionally, In the HFrEF group for the overall cohort, 81.0% were on triple therapy and 16.0% on quadruple therapy. Patient-reported QoL was worse in those with DM (median 68.1, IQR: 45.8 – 87.5) compared to those without DM (76.0, IQR: 53.1 – 92.7, $p < 0.001$, Figure 1C). When comparing patients based on ejection fraction only, QoL was significantly better in the heart failure with preserved ejection fraction (HFpEF) group compared to HFrEF and heart failure mildly reduced ejection fraction (HFmrEF) patients ($p < 0.001$, Figure 1D).

During a median follow-up time of 38.7 months (IQR: 30.7 – 48.2 months), patients with DM exhibited an increased risk of composite outcomes (aHR: 1.34, 95% CI 1.13 – 1.60, Figure 1E,G) and all-cause mortality alone (aHR: 1.12, 95% CI 1.01 –1.43, Figure 1F,G) compared to non-DM patients.

CONCLUSIONS
This study showcases that even with high rates of GDMT utilization in a contemporary specialized clinic, patients with concomitant HF and DM continues to experience poorer QOL and worse outcomes than HF patients without DM.

Table 1. Patient baseline characteristics and management of the HFC cohort (n=1301).

	Overall (n = 1301)		Without DM (n= 771)		With DM (n= 530)		p-value
Demographics							
Age (years)	66	(57-76)	65	(54-76)	69	(60-76)	p < 0.05
Sex (male)	911	(70.0 %)	519	(67.3 %)	390	(73.6 %)	p = 0.14
Ethnicity							
White	1104	(84.9 %)	675	(87.5 %)	429	(80.9 %)	p = 0.10
Indigenous	28	(2.2 %)	12	(1.6 %)	16	(3.0 %)	p = 0.05
Latin America	17	(1.3 %)	11	(1.4 %)	6	(1.1 %)	p = 0.32
Black	17	(1.3 %)	10	(1.3 %)	7	(1.3 %)	p = 0.49
Middle Eastern	21	(1.6 %)	12	(1.6 %)	9	(1.7 %)	p = 0.42
Asian	75	(5.8 %)	33	(4.3 %)	42	(7.9 %)	p < 0.05
Unknown	39	(3.0 %)	18	(2.3 %)	21	(4.0 %)	p = 0.06
Etiology							
IHD	427	(32.8 %)	206	(26.7 %)	221	(41.7 %)	p < 0.001
Non-IHD	874	(67.2 %)	565	(73.3 %)	309	(58.3 %)	p < 0.001
Medical History							
Hypertension	714	(54.7 %)	338	(43.8 %)	374	(70.6 %)	p < 0.001
Atrial Fibrillation	456	(35.0 %)	260	(33.7 %)	196	(37.0 %)	p = 0.17
CKD	439	(33.7 %)	202	(26.1 %)	237	(44.7 %)	p < 0.001
Cancer	385	(29.6 %)	208	(27.0 %)	177	(33.4 %)	p < 0.05
COPD	287	(22.1 %)	150	(19.5 %)	137	(25.8 %)	p < 0.01
DLP	304	(23.4 %)	130	(16.9 %)	174	(32.8 %)	p < 0.001
Devices							
PM	165	(12.6 %)	94	(12.2 %)	70	(13.2 %)	p = 0.31
ICD	278	(21.4 %)	142	(18.4 %)	136	(25.7 %)	p < 0.001
CRT	63	(4.8 %)	33	(4.3 %)	29	(5.7 %)	p = 0.14
Baseline Medications							
ACEi/ARB/ARNI	1144	(87.9 %)	674	(87.4 %)	470	(88.7 %)	p = 0.41
Beta-blocker	1165	(89.5 %)	677	(87.8 %)	488	(92.1 %)	p = 0.21
MRA	830	(63.8 %)	471	(61.1 %)	359	(67.7 %)	p = 0.07
Insulin	168	(12.9 %)	0	(0.0 %)	168	(31.7 %)	p < 0.001
Metformin	278	(21.4 %)	2	(0.3 %)	274	(51.7 %)	p < 0.001
SGLT2i	92	(7.1 %)	1	(0.1 %)	91	(17.2 %)	p < 0.001
Sulfonylurea	93	(7.1 %)	0	(0.0 %)	93	(17.5 %)	p < 0.001
GLP-1/DPP IV	34	(2.6 %)	2	(0.3 %)	32	(6.0 %)	p < 0.001

Laboratory markers							
BNP (ng/L)	440	(172-976)	401	(157-898)	502	(198-1078)	$p < 0.05$
HbA1c (%)	6.3	(5.8-7.3)	5.8	(5.5-6.1)	7.1	(6.5-8.2)	$p < 0.001$
Creatinine (umol/L)	102	(83-130)	96	(80-119)	114	(89-146)	$p < 0.001$
ACR (mg/mmol)	2.96	(0.8-15.4)	1.59	(0.45-8.20)	3.96	(0.97-16.46)	$p < 0.01$
Hemoglobin (g/L)	133	(119-146)	136	(122-148)	129	(115-129)	$p < 0.001$
Cholesterol (mmol/L)	3.65	(3.09-4.61)	3.94	(3.27-4.83)	3.40	(2.94-4.23)	$p < 0.001$
CKD-Epi ($mL/min/1.73m^2$)	61	(43-80)	65	(48-82)	52	(37-72)	$p < 0.001$
Echocardiogram							
EF (%)	40.7	(30.4-52.5)	41.1	(31.1-52.5)	40.3	(30.0-52.5)	$p = 0.24$
HFrEF (≤40%)	626	(48.1 %)	365	(47.3 %)	261	(49.2 %)	$p = 0.38$
HFmrEF	262	(20.1 %)	143	(18.5 %)	119	(22.5 %)	$p = 0.08$
HFpEF (≥50%)	389	(29.9 %)	245	(31.8 %)	144	(27.2 %)	$p < 0.05$

Values are given as n (%) or median (interquartile range). P-value column is comparing the cohort with Diabetes vs without Diabetes. A1C, glycated hemoglobin; ACEi, angiotensin-converting enzyme inhibitors; ACR, albumin-to-creatinine ratio; ARB, angiotensin receptor blockers; ARNI, angiotensin receptor/neprilysin inhibitor; BNP, brain natriuretic peptide; CKD, chronic kidney disease; CKD-Epi, equation used to calculate glomerular filtration rate; COPD, chronic obstructive pulmonary disease; CRT, cardiac re-synchronization therapy; DLP, dyslipidemia; DPP IV, dipeptidyl peptidase 4; EF, ejection fraction; GLP-1, glucagon-like peptide 1; HFmrEF, heart failure with mildly reduced ejection fraction; HFpEF, heart failure with preserved ejection fraction; HFrEF, heart failure with reduced ejection fraction; ICD, implantable cardioverter defibrillator; IHD, ischemic heart disease; MRA, mineralocorticoid receptor antagonist; PM, pacemaker; SGLT2i, sodium-glucose transporter 2 inhibitor.

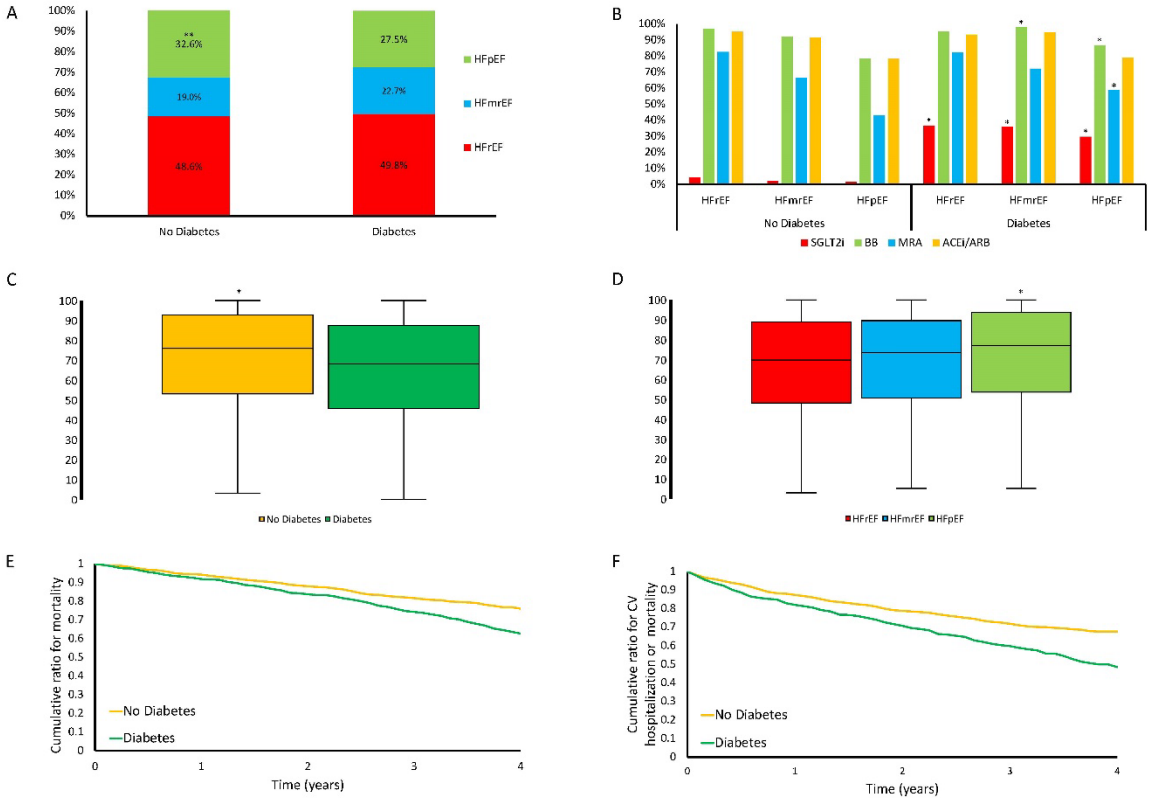

G

	HR	p-value	(95% CI)	aHR	p-value	(95% CI)
Mortality	1.43	(<0.001)	1.16-1.78	1.36	(0.006)	1.09-1.69
CV hospitalization or mortality	1.34	(<0.001)	1.13-1.60	1.12	(0.046)	1.01-1.43

Figure Legend

Figure 1. Clinical features, quality of life and clinical outcomes of patients based on their diabetes status in the HFC registry. (A) Distribution of EF based on Diabetes or no Diabetes status. (B) GDMT drug utilization for different EF based on diabetes or no diabetes status. (C) KCCQ-12 score based on diabetes or no diabetes. (D) KCCQ-12 score based on LVEF categories. (E) Kaplan-Meier analysis of all-cause mortality alone (log rank $P < 0.001$). (F) Kaplan-Meier analysis of CV hospitalization or mortality (log rank $P < 0.001$). (G) Multivariable Cox regression analysis of composite clinical outcomes adjusted and unadjusted hazard ratio for patients in the HFC registry with and without DM. * = p value < 0.001 when comparing the cohort with diabetes to without for (B) and (C), and when comparing to the other sub-groups in (D), ** = p value < 0.05, when comparing the cohort with diabetes to without for (A), ACEi/ARB = Angiotensin-converting enzyme inhibitors, angiotensin II receptor antagonists and angiotensin II receptor antagonist/neprilysin inhibitor, aHR = adjusted hazard ratio, BB = Beta-blocker, EF = ejection fraction, HR = unadjusted hazard ratio, HFmrEF = heart failure with mildly-reduced ejection fraction, HFrEF = heart failure with reduced ejection fraction, HFpEF = heart failure with preserved ejection fraction, MRA = mineralocorticoid receptor antagonist.

Session 3, Cardiac Function oral presentation

Hyperkalemia-related heart failure therapy discontinuation and its association with adverse outcomes in patients with heart failure: a population-based study

Aanchel Gupta, Sunjidatul Islam, Douglas Dover, Padma Kaul, Finlay McAlister, Justin Ezekowitz

BACKGROUND
Renin–angiotensin–aldosterone system (RAAS) inhibitors are evidence-based therapies in patients with heart failure (HF), but their use is often limited by episodes of hyperkalemia.

METHODS/RESULTS
A population-based cohort study in patients who were hospitalized or presented to the emergency department in Alberta with HF and experienced RAASi-induced hyperkalemia between April 2012 and March 2020. Episodes of hyperkalemia were identified from all potassium (K>5.0 mmol/L) measurements available. Patients were followed for 30 days following the hyperkalemia episode to determine whether their RAAS was dose-changed, discontinued, or maintained. Overall, 7,527 patients (median age of 79 years, 54.7% men) with heart failure had RAASi-associated hyperkalemia over 123,038 RAASi-treatment years (17 events per 100 RAASi-treatment years) and 73.4% had serum K<5.5 mEq/L. The development of hyperkalemia led to the discontinuation of RAASi in 35.2% of episodes, down-titration in 8.4%, and continuation in 56.4%. Discontinuation or down-titration of RAASi was more common when serum potassium exceeded 6.0 mEq/L (49.4%) than when serum K was 5.5-6.0 mEq/L (37.2%) or 5.0-5.4 (33.8%). Over a median follow-up of 1.4 years, discontinuation or down-titration of RAASi was associated with increased risk of all-cause mortality (aHR 1.80), hospitalizations for cardiovascular disease (aHR 1.09), and ED visits for heart failure (aHR 1.17) as compared to the continuation of RAASi therapy.

CONCLUSIONS
In patients with heart failure, RAASi discontinuation or down-titration was associated with higher mortality and cardiovascular events compared to continuation of RAASi therapy, even after inverse probability weighting. Developing strategies to maintain RAASi treatment after hyperkalemia events may improve clinical outcomes in heart failure patients.

Session 1, Recovery of Function oral presentation

Safety and Efficacy of Inclisiran in a Real-World Canadian High-Risk Population

Noah Hatch LPN, Jenna Knight BScN, RN, Cecily Hidson, BScN, RN, Bradley Brochu, MD, Sudheer Sharma, MD, Ben Tyrrell, MD, Tyler Lamb, MD, Neil Brass, MD, Debraj Das, MD, Micha Dorsch, MD

BACKGROUND
Lowering LDL cholesterol reduces cardiovascular events. However, numerous high-risk patients do not achieve guideline informed targets. Inclisiran is a novel small interfering RNA molecule that significantly lowers LDL by inhibiting the hepatic expression of PCSK-9. The purpose of this study is to describe the initial experience with this recently approved drug in a Canadian real-world population of high-risk patients.

METHODS/RESULTS
In a private-public partnership, the Royal Alexandra Hospital Foundation, Edmonton Cardiology Consultants, and Novartis Pharmaceuticals initiated a multidisciplinary team to operate a Risk Reduction Clinic. It is run through a large private metropolitan cardiology office focusing on secondary prevention and high-risk primary prevention patients. Patients are referred by their Cardiologists. All modifiable risk factors are addressed. Relevant demographic, clinical and outcome characteristics for all consecutive patients are prospectively captured in a purpose-built database.

From January 10, 2023, to April 22, 2024, 623 patients were assessed in this Clinic, of whom 307 (49.3%) patients did not meet their LDL target. After adjustment of lifestyle and other pharmacotherapy, 126 patients met the requirements to initiate Inclisiran; of those 110 were treated for secondary prevention and 16 patients for heterozygous familial hyperlipidemia. The mean age of patients started on inclisiran was 62 (12.5) years. 35% of patients were female. 61% of patients were on high dose statin and 39% were on low dose statin. 63% of patients were on ezetimibe. Mean LDL prior to inclisiran initiation was 2.84 mmol/L (1.00). 95 patients had a repeat lipid profile after their first inclisiran dose. For those mean LDL was 1.29 mmol/L (SD 0.86), representing a 54.6% reduction. This allowed 79%of patients to get to their LDL target. The LDL lowering effect was preserved up to 9 months (graph1). Non-HDL was reduced in a similar fashion, other lipid parameters were not affected by inclisiran (table1). Side effects reported were limited to local injection site reactions including redness, bruising, and tenderness. Four patients discontinued inclisiran; two patients no longer qualified because they were unable to take statins, one deceased, and one no longer wanted to be enrolled in the patient support program.

CONCLUSIONS
In this real-world, high risk Canadian population inclisiran is well tolerated and effectively reduces LDL cholesterol allowing 79% of patients to achieve their lipid target. In line with other reports, we saw a small reduction in Lp(a) after treatment with Inclisiran.

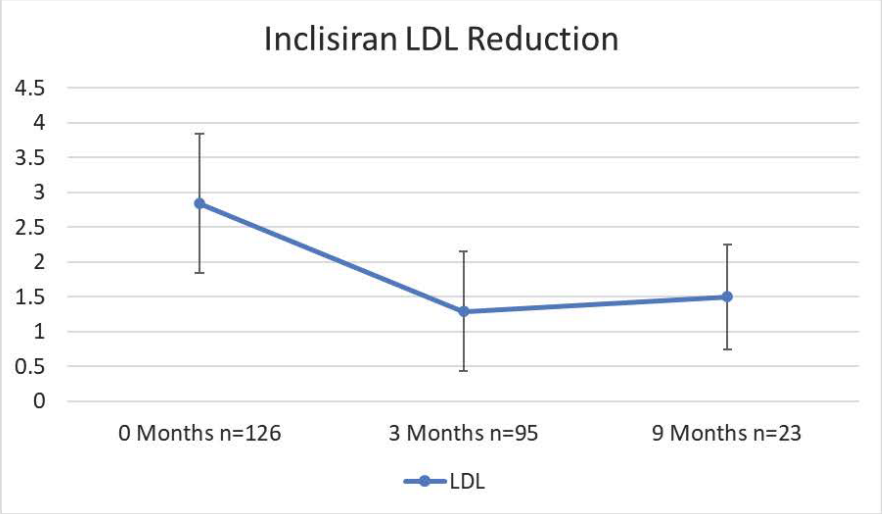

	Before Inclisiran	After Inclisiran	P Value
LDL (mmol/l)	2.84 (1.00) n=126	1.29 (0.86) n=95	<.001
n-HDL (mmol/l)	3.59 (1.11) n=125	1.89 (0.94) n=95	<.001
Triglycerides (mmol/l)	1.67 (0.95) n=126	1.64 (1.21) n=96	.613
Lp(a) (nmol/l)	137 (114) n=114	124 (133) n=95	.007

Poster #8

Investigating the sexual dimorphism in isoproterenol-induced cardiac hypertrophy in Sprague Dawley rats

Sara Helal, Samar Gerges, Sareh Panahi, Jason Dyck, Ayman El-Kadi

BACKGROUND
Distinct differences between sexes exist in various cardiovascular diseases, with women exhibiting a lower prevalence compared to men in numerous instances. Moreover, there is a significant correlation between the pathogenesis of cardiac hypertrophy and the metabolites of arachidonic acid (AA) mediated by cytochrome P450 (CYP) enzymes. The potential link between these sex differences and the expression and/or activity of CYP and their AA-mediated metabolites remains to be elucidated.

METHODS/RESULTS
Methods: Male and female Sprague-Dawley rats were subjected to i.p. injection of 1 mg/kg isoproterenol (ISO) daily for seven consecutive days to induce cardiac hypertrophy. Echocardiography (ECHO) was conducted before and after the induction of cardiac hypertrophy. Gene and protein expression of hypertrophic markers as well as various CYP enzymes in the heart tissues were determined by real-time PCR and Western blot analysis, respectively. Heart microsomal protein from control and ISO-treated rats was incubated with AA. Thereafter, the formed AA metabolites were determined by liquid chromatography-tandem mass spectrometry.
Results: Both sexes showed a significant degree of cardiac hypertrophy as proved by the ECHO with varying levels. Heart weight/Tibial length and left ventricular mass and diameters were significantly higher in male compared to female rats. In addition, the β/α -myosin heavy chain hypertrophic marker is twofold higher in male compared to female rats. Albeit the 20-hydroxy eicosatetraenoic acid (20-HETE) metabolite formation showed an almost equal increase in both sexes, the mid-chain HETEs (5, 12, and 15-HETE) were higher in male rats which parallel the increase in the gene and protein level of CYP1B1. The formation rate of the epoxyeicosatrienoic acids (EETs) was almost normal in the treated female rats compared to the control, while it decreased significantly in the male rats.

CONCLUSIONS
Our results suggest sexual dimorphism in the ISO-induced cardiac hypertrophy in rats specifically on the level of CYP enzymes and their AA-mediated metabolites.

Support: This work was supported by a grant from the Canadian Institutes of Health Research [CIHR PS 168846] to A.O.S.E-K. S.H. is the recipient of the Egyptian Government Scholarship.

Poster #9

An Optimized a Chiral Liquid Chromatography – Electrospray Ionization-Tandem Mass Spectrometry (LC-ESI-MS/MS) Ionization Method for the Enantioselective Determination of Underived Epoxyeicosatrienoic acids (EETs).

Fadumo Ahmed Isse, MSc, Ayman O. S. El-Kadi, PhD, Ahmed A. El-Sherbeni, PhD

BACKGROUND
Cytochrome P450 (CYPs) are become the hotspot of the research involving cardiovascular disease as CYP metabolic pathway of AA results in vasodilator and anti-inflammatory eicosanoids called epoxyeicosatrienoic acids (EETs). The current reported chiral LC-MS/MS assays have either a long run time (about 100 min) or there is a derivatization step involved in the process of EET quantification, adding further complexity, therefore, the objective of current assay was to develop and validate a chiral assay for quantitation of underived EET enantiomers using Liquid Chromatography Mass Spectrometry (LC-MS/MS) with a short run time

METHODS/RESULTS
A specific mass transition was scanned for each EET regio-isomer by obtaining a unique multiple reaction monitoring (MRM). MS parameters such as the collision energy and the ionization polarity were optimized. The operational condition for liquid chromatography involved using suitable mobile phases consisting of organic phase: acetonitrile, methanol, and isopropyl alcohol. EETs separation was performed using a chiral reverse phase REFLEC C-AMYLOSE column and a gradient elusion method. Other optimized parameters include flow rate, injection volume and the condition state of column.

CONCLUSIONS
The method achieved efficient separation of the two enantiomers for each 4 regio-isomer EETs. The linearity of the calibration curves over the range used (10-600 ng/ml) was > 0.99. The intra-run percent error and coefficient of variation (CV) were ≤ ± 15 %. The inter-run percent error and coefficient of variation (CV) were ≤ ± 15 %, and ≤ 15 %, respectively. The lowest quality control CV was < 20 %. The run time was 20 minutes. Conclusion: This LC-ESI-MS/MS chiral assay shows promise for measuring underived EETs with a short run time. The method was found to be accurate and precise in measuring the spiked standard EETs.

Session 2, Vascular Function oral presentation

The Role of VSMC MMP14 in The Development of Atherosclerosis

Suha Jarad, Ziyang Zhang, Hongmei Gu, Govind Gill, Peter Amadi, Dawei Zhang

BACKGROUND
Vascular smooth muscle cells (VSMCs) are essential contributors in atherosclerotic plaques development; however, to develop a foam cell, VSMCs need to migrate from their original place in the medial layer of the artery to the intimal layer. This requires degrading the surrounding extracellular matrix (ECM) components like collagen and fibronectin by proteases. Membrane type-1 matrix metalloproteinase or MMP14 has a role in ECM degradation and it also plays an important role in atherosclerosis and promotes cell migration/invasion in VSMCs. Here, we investigate the role of MMP14 on atherosclerosis development and VSMC migration/ invasion utilizing in-vivo and in-vitro approaches.

METHODS/RESULTS
We developed tamoxifen-inducible SMC-specific Mmp14 knockout mice using the Cre-Lox technique. We found that SMC Mmp14 knockout had no significant effect on baseline cardiac function, body weight, or lipid profile. Primary VSMCs were isolated from the aorta and utilized to confirm that MMP14 expression was effectively reduced in SMC-specific Mmp14 knockout mice. MMP14 knockdown in cultured human artery smooth muscle cells (HASMCs) significantly reduced HASMC migration and invasion through the collagen I barrier, confirming MMP14's role in VSMC migration/invasion.
To assess atherosclerosis development, we induced SMC-specific Mmp14 knockout in adult Ldlr-/- mice. Mice were then fed a high-fat/high-cholesterol diet for 16 weeks to develop atherosclerosis. We found that mice lacking VSMC Mmp14 showed a significant reduction in atherosclerotic plaques but displayed no significant difference in lipid profile or body weight compared to control mice.

CONCLUSIONS
SMC Mmp14 knockout didn't affect the cardiac function or lipid profile in mice but significantly reduced atherosclerosis development. Since MMP14 promotes VSMC migration/invasion, understanding the molecular mechanisms of how MM14 modulates this process and promotes atherosclerosis progression will pave the way for possible therapeutic targets to ameliorate atherosclerosis development.

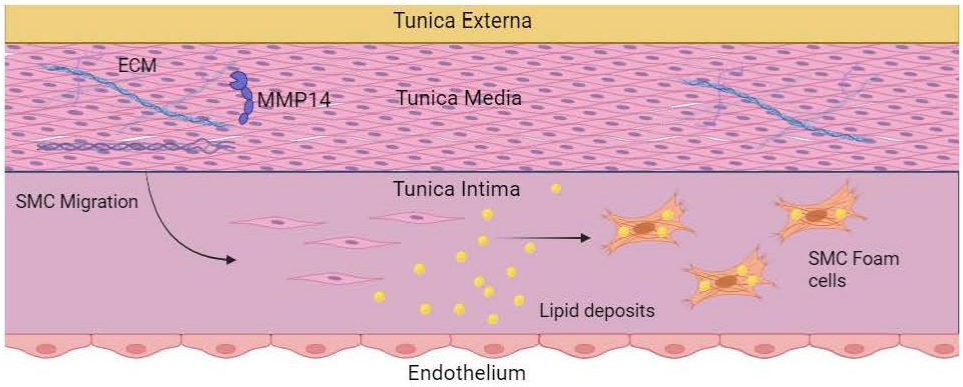

Session 2, Vascular Function oral presentation

SIRT2 Inhibition Decreases Glycolysis and Attenuates Hypertrophic Response in H9c2 Cardiomyocytes

Ezra B. Ketema, Muhammad Ahsan, Kaya Persad, Qiuyu Sun, Liyan Zhang, Gary D. Lopaschuk

BACKGROUND
Myocardial glycolysis increases in hypertrophic and failing hearts. Hyperacetylation also occurs in the failing heart, and many glycolytic enzymes are known to undergo acetylation modifications. However, it is generally considered that acetylation has inhibitory effects on glycolysis. As a result, it is not clear whether acetylation changes directly contribute to glycolysis changes in cardiac hypertrophy. We, therefore, determined whether changes in the acetylation of glycolysis enzymes and the activity of the cytosolic deacetylase SIRT2 regulate cardiac glycolysis.

METHODS/RESULTS
Methods: Glycolysis rates were directly measured in rat heart-derived H9c2 cardiomyocytes perfused with 5 mM [5-3H]glucose, 0.8 mM palmitate, and 4% bovine serum albumin. Before these metabolic measurements, H9c2 cells were treated with either a SIRT2 inhibitor (10 μM AGK2) or a vehicle for 24 hours. In separate experiments, SIRT2 was also knocked down in H9c2 cells using siRNA, followed by glycolysis rate determinations. The impact of SIRT2 inhibition or SIRT2 knockdown on overall or glycolytic enzyme acetylation was also assessed. Furthermore, the effects of SIRT2 inhibition on hypertrophic signalling were assessed by treating H9c2 cells with phenylephrine.

Results: SIRT2 inhibition markedly decreased glycolysis rates in H9c2 cells compared to vehicle-treated cells (524±108 vs 2631±372 nmol.g dry wt-1.min-1, $p<0.05$). Similarly, SIRT2 knockdown resulted in a significant reduction in glycolysis rates compared to scrambled siRNA-treated H9c2 cells (745±31 vs 1659±168 nmol.g dry wt-1.min-1, $p<0.05$). The decrease in SIRT2 was accompanied by an increase in the acetylation status of the glycolytic enzyme glyceraldehyde phosphate dehydrogenase (GPDH). Moreover, a trend towards increased phosphofructokinase (PFK) acetylation was also observed in SIRT2 knockdown H9c2 cells compared to scrambled siRNA-treated cells. Lastly, AGK2 treatment also attenuated phenylephrine-mediated hypertrophic responses in H9c2 cells.

CONCLUSIONS
Increased acetylation of glycolytic enzymes is associated with a decrease in glycolysis, and SIRT2 inhibition or deletion in H9c2 cells significantly decreases glycolysis rates and attenuates hypertrophy. SIRT2 may, therefore, contribute to the increased glycolysis seen in hypertrophy and heart failure.

Poster #10

Personalized Treatment Recommendations for Coronary Artery Disease Patients: Comparing PCI vs CABG through Individual Survival Distributions

Anita Khalafbeigi, Sunil V Kalmady, Kevin Bainey, Robert Welsh, Padma Kaul, Russell Greiner

BACKGROUND
Applied AI in healthcare holds promise for personalized treatment recommendations by analyzing vast datasets and patterns. While many projects focus on estimating counterfactual outcomes and individual treatment effects (ITE) using binary clinical outcomes like 30-day mortality or disease relapse, few consider more general time-to-event outcomes. Individual Survival Distribution (ISD) models offer probabilities of the event of interest at each future time for each instance. Unlike single-value risk scores, ISDs can capture temporal variations in survival probabilities, providing insight into how a patient's condition changes with respect to their features and treatment received, facilitating individualized treatment planning.

METHODS/RESULTS
This study focuses on predicting ISDs for mortality associated with different treatment types (for the same individual) to compare their effects. We applied this methodology to a large-scale real-world observational dataset of patients with coronary artery disease from 2002 to 2019, comparing percutaneous coronary intervention (PCI) versus coronary artery bypass grafting (CABG) on an individual basis. This dataset includes 107,916 patients, with 85,706 patients receiving PCI and the remainder undergoing CABG. We know the time of death for 23.14% of the patients; the remaining 76.86% are "censored" – either because they left the study or were known to be alive when the study ended. The dataset includes information collected during the diagnosis and cardiac catheterization process, along with demographics and event status (death), resulting in 150 features. The data is divided into training and test sets in a 80:20 ratio, ensuring unique patients in each set.
We applied the Neural Multi-Task Logistic Regression (N-MTLR) system to learn a model that can predict ISDs with error bars for each treatment for each patient. Model performance was evaluated on the test set using factual outcomes, resulting in a C-index of 0.772 ± 0.003 and an Integrated Brier Score (IBS) of 0.125 ± 0.001. Among 23,475 patients in the holdout set, our learned model claimed that CABG was (statistically significant) better than PCI for 4,998 patients, and PCI was better than CABG for 16,433 patients, in terms of the mean survival time (paired t-test, $P < 0.05$).

CONCLUSIONS
This study explored the efficacy of ISD methods, particularly the N-MTLR, in comparing mean survival times across various treatments for individuals. N-MTLR offers a nuanced analysis, capturing complexities like crossing survival curves, unlike methods like CoxPH which rely on proportionality assumptions. For future direction, we aim to apply different techniques to reduce selection bias, enhancing the reliability of counterfactual estimations.

Poster #11

Variation in risk-adjusted cardiac intensive care unit (CICU) length of stay and the association with in-hospital mortality

Koerber DM, Katz JN, Bohula E, Park JG, Dodson MW, Gerber DA, Hillerson D, Liu S, Pierce MJ, Prasad R, Rose SW, Sanchez PA, Shaw J, Wang J, Jentzer JC, Kristin Newby L, Daniels LB, Morrow DA, van Diepen S

BACKGROUND

Background: Previous studies have suggested that there is wide variability in cardiac intensive care unit (CICU) length of stay (LOS); however, these studies are limited by the absence of detailed risk assessment at the time of admission. Thus, we evaluated inter-hospital differences in CICU LOS, and the association between LOS and in-hospital mortality.

METHODS/RESULTS

Methods: Using data from the Critical Care Cardiology Trials Network (CCCTN) registry, we included 22,862 admissions between 2017 and 2022 from 35 primarily tertiary and quaternary CICUs that captured consecutive admissions in annual 2-month snapshots. The primary analysis compared inter-hospital differences in CICU LOS, as well as the association between CICU LOS and all-cause in-hospital mortality using a Fine and Gray competing risk model.

Results: The overall median CICU LOS was 2.2 (1.1-4.8) days, and the median hospital LOS was 5.9 (2.8-12.3) days. Admissions in the longest tertile of LOS tended to be younger with higher rates of pre-existing comorbidities, and had higher Sequential Organ Failure Assessment (SOFA) scores, as well as higher rates of mechanical ventilation, intravenous vasopressor use, mechanical circulatory support, and renal replacement therapy. Unadjusted all-cause in-hospital mortality was 9.3%, 6.7%, and 13.4% in the lowest, intermediate, and highest CICU LOS tertiles. In a competing risk analysis, individual patient CICU LOS was correlated ($r^2 = 0.31$) with a higher risk of 30-day in-hospital mortality. The relationship remained significant in admissions with heart failure, ST-elevation myocardial infarction and non-ST segment elevation myocardial infarction.

CONCLUSIONS

Conclusions: In a large registry of academic CICUs, we observed significant variation in CICU LOS and report that LOS is independently associated with all-cause in-hospital mortality. These findings could potentially be used to improve CICU resource utilization planning and refine risk prognostication in critically ill cardiovascular patients.

Poster #12

Establishing a Direct Interaction Between the 19,20-EDP Analog SA-22 and SIRT3: Impact on Cardiac Mitochondrial Homeostasis

Joshua Kranrod, Robert Valencia, Ahmed Darwesh, Marawan Ahmed, Mobina Heidari, Adeniyi Michael Adebesin, Sailu Munnuri, Khaled Barakat, John Falck, John Seubert

BACKGROUND
Despite extensive study, the structural, metabolic, and mechanistic heterogeneity amongst polyunsaturated fatty acids (PUFA) has confounded identification of their molecular targets and roles in cardiovascular diseases. Previously our group demonstrated that the cardioprotective properties of both 19,20-epoxydocosapentaenoic acid (EDP), a CYP450-derived metabolite of docosahexaenoic acid (DHA), and a synthetic structural analog SA-22, were SIRT3-dependent. Thus, we investigated potential functional interactions between SA-22, SIRT3, and their impact on mitochondrial homeostasis in the context of hypoxic myocardial injury.

METHODS/RESULTS
In silico analysis of NAD+/SA-22/hSIRT3 complexes employed the Schrodinger Suite and AMBER18. SA-22 ligand binding was validated via SYPRO Orange thermal shift assay. SIRT3 catalytic activity was measured using an acetylated HDAC fluorogenic substrate assay. Point mutagenesis experiments confirmed the involvement of residue SER149. H9c2 cells were used as an in vitro model of hypoxia/reoxygenation (HR) injury. Cells were deprived of oxygen for 24 hours followed by a 6-hour reoxygenation period wherein cells were treated with either vehicle, 19,20-EDP (1 µM), or SA-22 (1 µM), either with the pan-sirtuin inhibitor nicotinamide (NAM) (30 µM), or the SIRT3-selective inhibitor 3-(1H-1,2,3-triazol-4-yl)-pyridine (3-TYP) (50 µM). Mitophagy was assessed via immunoblotting and the pH-dependent fluorescent mitophagy reporter protein (mito-Keima). Mitochondrial respiration was measured using high-resolution respirometry (Oroboros-O2K). SA-22 stabilized highly conserved residues adjacent to the nicotinamide-binding C-pocket and improved their binding affinities to NAD + in silico. Addition of SA-22 altered SYPRO Orange fluorescence and improved catalytic activity in vitro but was abrogated by SER149 substitution, indicating that SA-22 is a positive allosteric modulator of SIRT3. Lastly, SA-22 protected cardiac cells against HR-induced changes in mitophagy and mitochondrial respiration in a SIRT3-dependent manner.

CONCLUSIONS
SA-22 directly binds and enhances the activity of SIRT3, preserving cardiac mitochondrial homeostasis despite myocardial hypoxia-reoxygenation injury.

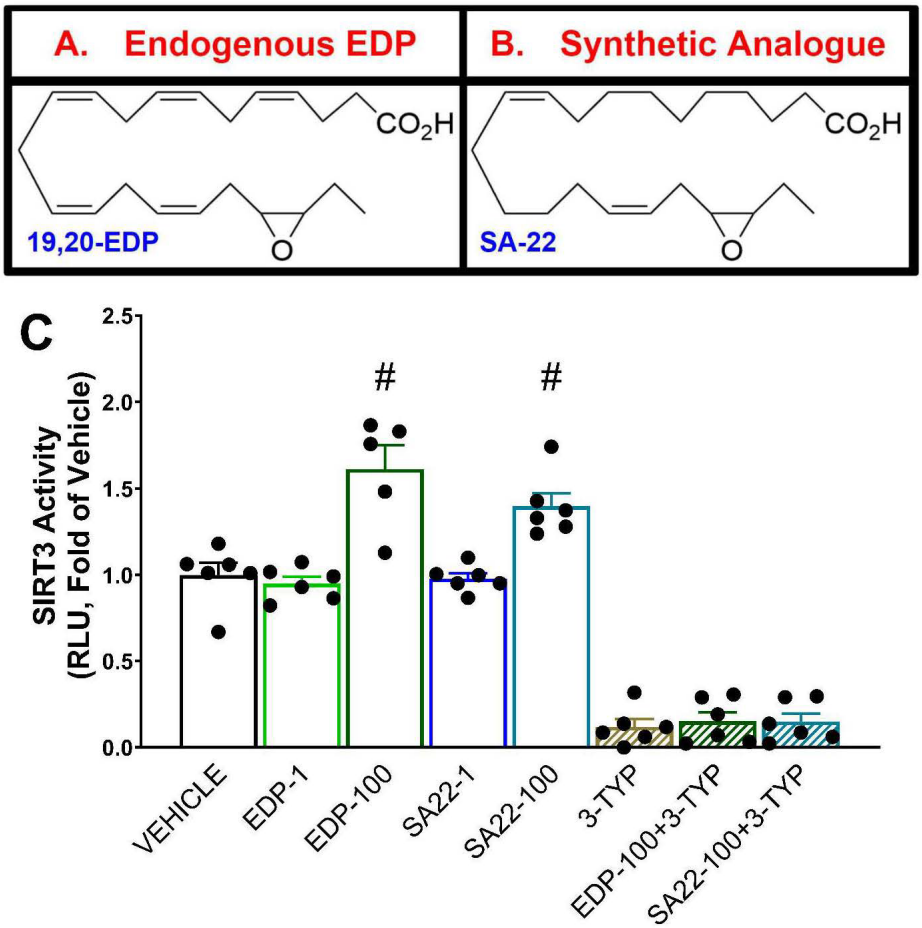

Figure 1. *SA-22 is a structural 19,20-EDP mimetic that boosts SIRT3 activity.* Chemical structures of an endogenously abundant metabolite of DHA, 19,20-EDP (A) as well as the metabolically more stable, synthetic analog SA-22 (B). (C) Human recombinant SIRT3 activity was assessed after incubation with either 19,20-EDP (1, 100 μM) or SA-22 (1, 100 μM), in the presence or absence of 3-TYP (50 μM) in vitro. Values represent mean ± SEM; # $p<0.05$ vs. VEHICLE (n = 5-6 per group). 3-TYP; 3-(1H-1,2,3-triazol-4-yl) pyridine, DHA; Docosahexaenoic acid, EDP; Epoxydocosapentaenoic acid, SA-22; (10Z,16Z)-18-(3-Ethyloxiran-2-yl)-octadeca-10,16-dienoic acid.

State	AERO	AERO SA-22	HR VEH-0H	HR VEH-3H	HR VEH-6H	HR SA-22-0H	HR SA-22-3H	HR SA-22-6H
Basal	49.24 ± 0.93	56.85 ± 1.95	21.98 ± 2.67	24.29 ± 2.25	25.14 ± 4.17	53.81 ± 2.45	58.01 ± 2.00	45.83 ± 3.12
PM_L (N_L)	18.67 ± 2.74	24.49 ± 1.88	11.11 ± 1.64	15.74 ± 2.70	14.16 ± 1.93	22.67 ± 1.50	15.12 ± 3.02	25.34 ± 1.24
PM_P (N_P)	49.37 ± 4.94	74.41 ± 6.24	20.11 ± 4.30	32.72 ± 3.88	28.53 ± 4.35	69.63 ± 4.41	44.18 ± 8.17	74.78 ± 6.24
PMC_P (N_P)	70.19 ± 7.25	100.68 ± 8.29	47.77 ± 11.98	48.28 ± 6.77	40.32 ± 4.95	84.52 ± 3.84	54.79 ± 9.40	78.31 ± 5.92
PMG_P (N_P)	70.06 ± 7.06	100.14 ± 8.53	35.40 ± 10.74	45.39 ± 6.39	48.85 ± 3.86	84.41 ± 4.83	80.65 ± 15.89	83.28 ± 11.16
$PMGS_P$ (NS_P)	116.91 ± 10.18	177.49 ± 6.81	70.31 ± 17.12	53.63 ± 7.11	80.87 ± 6.20	198.73 ± 20.21	198.83 ± 41.88	175.23 ± 11.75
$PMGS_E$ (NS_E)	178.21 ± 13.43	227.79 ± 27.75	79.06 ± 21.26	103.46 ± 20.49	119.54 ± 5.80	310.06 ± 26.37	299.82 ± 61.30	220.22 ± 33.93
$PMGS(Rot)_E$ (S_E)	8.73 ± 2.03	1.48 ± 0.36	20.98 ± 3.86	41.83 ± 8.78	31.05 ± 3.72	2.13 ± 0.99	5.43 ± 0.91	5.86 ± 2.03
ROX	6.05 ± 0.99	3.29 ± 0.62	1.71 ± 0.59	9.50 ± 1.85	6.46 ± 1.52	8.81 ± 0.98	5.82 ± 1.08	10.07 ± 1.53

Table 1. *Raw oxygen consumption rates in H9c2 cells treated with SA-22.* High-resolution respirometric assessment of H9c2 cells subjected to HR insult with or without SA-22 (1 µM) treatment. Following permeabilization with digitonin (4 µM), cells were analyzed with the SUIT-008 protocol. OCRs from each respiratory state were obtained by normalizing oxygen flux following each substrate titration to ROX; Basal, Pyruvate (5 µM) and Malate (2 µM) (PM_L), ADP (10 µM) (PM_P), Cytochrome c (10 µM) (PMC_P), Glutamate (10 µM) (PMG_P), Succinate (10 µM) ($PMGS_P$), FCCP (0.3 µM) ($PMGS_E$), Rotenone (0.5 µM) ($PMGS(Rot)_E$), and Antimycin A (2.5 µM) (ROX). Treatments; vehicle (0.1% v/v DMSO), SA-22 (1 µM). Values represent mean ± SEM (n = 4-18 per group). SA-22; (10Z,16Z)-18-(3-Ethyloxiran-2-yl)-octadeca-10,16-dienoic acid. FCCP; Carbonyl cyanide p-trifluoromethoxyphenylhydrazone. HR; hypoxia-reoxygenation. ROX; Residual Oxygen Consumption. P; Pyruvate. $_P$; ADP-stimulated respiration. M; Malate. G; Glutamate. S; Succinate. $_L$; LEAK. $_E$; Maximum uncoupled respiration. N; N-Pathway (i.e. Complex I). OCR; oxygen consumption rate. SUIT; Substrate-uncoupler-inhibitor titration

Poster #13

Investigating the Role of Ferroptosis in Neonatal Sepsis-Induced Liver Injury

Si Ning Liu, Jad-Julian Rachid, Danny Shimatu, Ben Magalnick, Kimberly Macala, Stephane Bourque

BACKGROUND
Late-onset-sepsis (LOS) is the dysregulated host response to an infection occurring after 72 hours of life. The Global Burden of Disease study estimates LOS affects 1.3 million neonates annually, with most cases occurring in low- and middle-income countries. Ferroptosis is an iron-dependent type of cell death that occurs following tissue iron sequestration, which is known to occur during inflammation. Given that the liver is a major organ for iron storage, we hypothesized that LOS-induced inflammation would induce ferroptosis, leading to liver dysfunction.

METHODS/RESULTS
Methods: Three-day-old Sprague Dawley pups received an intraperitoneal injection of fecal slurry (FS, 1.0 mg/g body weight) or vehicle (5% dextrose). All pups received buprenorphine for pain control and antibiotics with fluids. Pups were euthanized at 8h and 24h for blood and tissue collection. In another subgroup of pups, ferrostatin-1 (Fer-1, 1mg/kg in 0.3% DMSO in saline) or vehicle (0.3% DMSO in saline) was administered subcutaneously 24h and 1h before FS injection to assess the effectiveness of a ferroptosis-specific suppressor in improving liver function. Markers for liver stress (plasma ALT), lipid peroxidation (MDA), and Fe3+ levels were assessed using available kits; gene and protein expression profiles of mediators of ferroptosis were assessed by qPCR and Western blots, respectively. Results: FS caused 30% mortality in septic pups ($P<0.0001$). In surviving pups, IL-1β levels were increased, as were liver Fe3+ levels (+60%; $P<0.0001$), and plasma ALT levels (+840%; $P<0.0001$) at 24h post-FS injection. Malondialdehyde, a marker of lipid peroxidation, was increased 8h post FS injection (+230%;
$P=0.0005$). Transcript profiles of key regulators of ferroptosis, including glutathione peroxidase 4 (Gpx4) and ferroptosis suppressor protein (Fsp1), were downregulated (-42%, $P<0.0001$; -40%, $P=0.0003$; respectively) in septic pups at 24h post-FS. Pretreatment with Fer-1 did not affect survival in of septic pups, nor did it improve sepsis severity measured by the neonatal rat sepsis scores or plasma ALT levels.

CONCLUSIONS
Despite increased lipid peroxidation, tissue liver iron levels, and downregulation of Gpx4, pretreatment with Fer-1 did not improve liver function or survival outcomes, suggesting the degree of lipid peroxidation may not be severe enough to induce ferroptosis.

Session 4, 3MT-style presentation

The Sodium/Glucose Cotransporter 2 Inhibitor Empagliflozin Inhibits Long QT 3 Late Sodium Currents in a Mutation Specific Manner

Lynn C. Lunsonga, Mohammad Fatehi, Wentong Long, Amy J. Barr, Brittany Gruber Arkapravo Chattopadhyay, Khaled Barakat, Andrew G. Edwards and Peter E. Light

BACKGROUND
Sodium/glucose cotransporter 2 inhibitors (SGLT2is) such as empagliflozin have demonstrated substantial cardioprotective effects in patients with or without diabetes. The SGLT2is have been shown to selectively inhibit the late component of cardiac sodium current (late INa). Induction of late INa is also the primary mechanism involved in the pathophysiology of congenital long QT syndrome type 3 (LQT3) gain-of-function mutations of the major cardiac sodium channel isoform Nav1.5. Therefore, we investigated the effect of empagliflozin on late INa in thirteen known LQT3 mutations located in distinct regions of the channel structure.

METHODS/RESULTS
The whole-cell patch-clamp technique was used to investigate the effect of empagliflozin (10 μM) on late INa in recombinantly expressed Nav1.5 channels containing different LQT3 mutations. Molecular modeling of human Nav1.5 and simulations in a mathematical model of human ventricular myocytes were used to extrapolate our experimental results to excitation contraction coupling. Empagliflozin selectively inhibited late INa in LQT3 mutations residing in the inactivation gate region of Nav1.5, with no effect on peak current or channel kinetics. In contrast, empagliflozin caused inhibition of both peak and late INa in mutations in the S4 voltage-sensing regions. Empagliflozin had no effect on late/peak INa or channel kinetics in channels containing LQT3 mutations located in the putative empagliflozin binding region. Simulation of our experimental findings in a mathematical model of human ventricular myocytes predicts that empagliflozin may have a desirable therapeutic effect in LQT3 mutations located in the inactivation gate region.

CONCLUSIONS
Our results show that empagliflozin selectively inhibits late INa, without affecting gating kinetics, in LQT3 mutations residing in the inactivation gate region. The SGLT2is may therefore be a promising novel precision medicine approach for patients with certain LQT3 mutations.

Poster #14

Oxidative stress induced S-Glutathionylation of Myosin Light Chain 3 and Alpha Actinin 2 results in their unfolding and enhanced susceptibility to proteolysis

Zabed Mahmud1, Wesam Bassiouni2, Nish Rathod3, Philip B. Liu3, Howard Young3, Peter Hwang,3,4, and Richard Schulz1,2*

Departments of Pediatrics1, Pharmacology2, Biochemistry3, and Medicine4 University of Alberta, Edmonton, AB, Canada

BACKGROUND
Proteolytic degradation of cardiac sarcomeric proteins like myosin light chain 1 (MYL3) and alpha actinin 2 (ACTN2) by intracellular proteases during myocardial ischemia and reperfusion injury is well established. These proteins are crucial for sarcomeric function, yet, how they become targets for intracellular proteases like matrix metalloproteinase-2, calpain 1/2 and caspase-3 during ischemia and reperfusion injury remain elusive. Despite their high α-helical content and well-folded structures, MYL3 and ACTN2 might unfold due to oxidative stress-induced modifications like S-glutathionylation, as both contain three and ten cysteine residues, respectively. We hypothesized that S-glutathionylation could render MYL3 and ACTN2 more prone to proteolytic attack.

Our aim was to elucidate the molecular link between the oxidative modification of cysteine residues in MYL3 and ACTN2 and their unfolded/partially unfolded state prior to proteolysis.

METHODS/RESULTS
We explored the conditions leading to S-glutathionylation in MYL3 and ACTN2 using the thiol-reactive reagents S-nitroglutathione, glutathione disulfide, or glutathione in combination with diamide. We also developed a recombinant MYL346-195 chimeric protein fused with its binding partner MYH7776-810, and a truncated form of recombinant ACTN222-266 to conduct unfolding studies. Using mass spectrometry, we confirmed glutathionylation in conserved cysteine residues of both proteins induced by S-nitroglutathione. Circular dichroism, intrinsic fluorescence, and nuclear magnetic resonance studies revealed that glutathionylation caused a disturbance in the α-helical structure and tertiary conformation of MYL3 and ACTN2. Moreover, two-dimensional NMR experiments demonstrated a partial unfolded state of MYL3 and a complete unfolding state of ACTN2 following glutathionylation. Notably, both proteins showed increased susceptibility to trypsin-induced proteolysis upon glutathionylation.

CONCLUSIONS
In summary, we provide evidence suggesting that glutathionylation likely induces a conformational shift in MYL3 and ACTN2 in spite of their inherent stability, potentially exposing the cleavage sites for intracellular proteases. Our research highlights the impact of S-glutathionylation in determining the susceptibility of MYL3 and ACTN2 to protease-mediated cleavage, providing valuable insights into their vulnerability under oxidative stress conditions.

Poster #15

Cardiomyocyte-Specific ROMO1 Gene Delivery Lessens Mitochondrial Dysfunction and Promotes Angiogenesis in Mice with Heart Failure

Matthew D. Martens, Matthieu Zolondek, Heidi L. Silver, Mostafa Khairy, Daniela Morales-Lamas, Mourad Ferdaoussi, Helene Lemieux, and Jason R.B. Dyck

BACKGROUND
Although a vast array of pathophysiological and molecular events contribute to heart failure (HF), defects in cardiomyocyte mitochondrial metabolism have been shown to play a major role in the development and worsening of this disease. Recently, we identified the mitochondrial protein, reactive oxygen species modulator 1 (ROMO1), as an important regulator of cardiomyocyte mitochondrial function. We also showed that the expression of ROMO1 was significantly reduced in the failing human and mouse heart. Based on this, we set out to determine if restoring ROMO1 expression during the development of HF would be sufficient to improve both mitochondrial and cardiac contractile function to blunt heart failure progression in mice.

METHODS/RESULTS
Cardiomyocyte-specific gene delivery was achieved with control (AAV9-aMHC-Null) or ROMO1 (AAV9-aMHC-ROMO1) expressing viruses in male mice that underwent either sham control surgery or HF-inducing transverse aortic constriction (TAC) surgery. Echocardiographic analysis demonstrated that mice who received control virus following TAC had a characteristic 47.3% reduction in left ventricular ejection fraction (%EF), while mice that received ROMO1 virus following TAC only had a 26.7% reduction in %EF, compared to sham controls (n=18-29, $p<0.01$). High resolution respirometry of permeabilized cardiac fibers isolated from the hearts of all three experimental groups showed that TAC-induced HF significantly reduced mitochondrial oxidative phosphorylation compared to sham controls (n=5-8, $p<0.01$). However, ROMO1 rescue during TAC is sufficient to restore mitochondrial function back to sham control levels (n=5-8, $p<0.01$). This observation was supported by electron microscopy which revealed that ROMO1 expression during TAC prevented derangements in mitochondrial morphology and integrity that are typically observed in hearts from TAC-induced HF (n=3, $p<0.01$). Additionally, histological analysis indicated that cardiomyocyte-specific ROMO1 expression in mice with HF significantly increased the number of capillaries per cardiomyocyte compared to TAC alone (n=5, $p<0.01$). This increase in capillary/cardiomyocyte ratio was concurrent with a significant increase in cardiac vascular endothelial growth factor A (VEGF-A) mRNA and protein expression, compared to TAC alone (n=8-12, $p<0.05$), suggesting that ROMO1 expression also exerted beneficial effects by improving vascular perfusion for the hypertrophic cardiomyocyte.

CONCLUSIONS
Taken together, these data suggests that cardiomyocyte-specific ROMO1 expression not only directly regulates mitochondrial integrity and function, but also indirectly promotes VEGF-A production to stimulate increased capillary density, allowing for improved perfusion and blunted HF progression in mice.

Poster #16

Role of KCa channels and Connexin40 in ischemic-reperfusion injury in isolated rat hearts

C. McInroy, S.L. Gust, P.M. Kerr, R. Margaryan, F. Plane

BACKGROUND
Ischemic heart disease is a leading cause of death worldwide. Ischemia-reperfusion (IR) injury contributes to myocardial damage and subsequent heart failure. Thus, there is a clinical need to identify novel therapeutic targets. In this study, we have tested two hypotheses in isolated perfused rat heart:

1. Small molecule activators of cardiac mitochondrial small (SKCa) and intermediate conductance (IKCa) Calcium-activated K+ channels may prevent I/R injury.
2. Loss of Connexin40 (Cx40) will exacerbate I/R injury.

METHODS/RESULTS
Male Sprague Dawley rats, and male and female Cx40 knockout rats (Wistar background) were euthanized and hearts were rapidly excised, cannulated via the ascending aorta and perfused in Langendorff mode. Left ventricular pressure and heart rate were recorded and left ventricular developed pressure (LVDP) was calculated as the difference between left ventricular systolic pressure (LVSP) and LVEDP. Hearts were perfused under normoxic conditions for 30 minutes followed by global no-flow ischemia for 15 minutes. The hearts were then perfused aerobically for a further 45 minutes. Activators of SKCa and IKCa channels were added to the perfusate 10 minutes prior to induction of ischemia. Data were analysed using a two-way ANOVA was performed separately for pre- and post-ischemia.

Together, CyPPA and SKA-31 (both 10 μM), activators of SKCa and IKCa channels respectively, enhanced recovery following ischemia in isolated Sprague-Dawley rat hearts increasing post-ischemic LVDP from 6 ± 2 to 73 ± 2 mmHg ($P<0.01$; n=6). This effect was reduced by inhibitors of SKCa and IKCa channels but post-ischemic LVDP was still significantly greater than control at 44 ± 4 mmHg ($P<0.01$; n=6). In isolated hearts from both male and female rats lacking Cx40, post-ischemic functional recovery was significantly impaired compared to controls: 1 ± 2 and 16 ±3 compared to 24 ± 2 and 35 ± 4 mmHg, respectively (n=5-15).

CONCLUSIONS
We have shown that small molecule activators of SKCa and IKCa channels may protect against IR injury in isolated perfused hearts whereas loss of Cx40, a protein which mediates cellular electrical coupling, exacerbates IR damage. This study provides new insights into potential therapeutic targets to protect against IR injury in the heart.

Session 4, 3MT-style presentation

Sex-dependent changes of cardiac cytochrome P450 enzymes and hydroxyeicosatetraenoic acids in pressure overload-induced cardiac hypertrophy in rats

Samar H. Gerges, Sara A. Helal, Heidi L. Silver, Jason R.B. Dyck, and Ayman O.S. El-Kadi

BACKGROUND
Cardiac hypertrophy develops in response to stimuli such as pressure overload. It is a serious condition that could progress to heart failure, which is a very common disease in Canada. Cardiac hypertrophy is usually less common and has better prognosis in women than in men. Cytochrome P450 (CYP) enzymes are expressed in the heart and play an important role in the cardiovascular health. Some CYP enzymes like CYP1B1, CYP4A, and CYP4F enzymes metabolize arachidonic acid into several hydroxyeicosatetraenoic acids (HETEs), most of which have prohypertrophic effects. In this study, we investigated sex-specific differences in pressure overload-induced cardiac hypertrophy and its effect on the levels of cardiac CYP enzymes and HETEs.

METHODS/RESULTS
Methods: Adult male and female Sprague-Dawley rats were subject to sham or abdominal aortic constriction (AAC) surgeries to induce pressure overload-induced cardiac hypertrophy. Five weeks later, cardiac function was assessed by echocardiography and heart-weight-to-tibial-length (HW:TL) ratio was calculated. The mRNA of hypertrophic markers like atrial and brain natriuretic peptide (ANP and BNP), skeletal muscle α-actin (SkM α-actin), and β/α-myosin heavy chain (β/α-MHC) were measured by real-time PCR (RT-PCR). In addition, the mRNA and protein levels of different CYP enzymes were measured by RT-PCR and Western blot techniques, respectively. Heart microsomes were incubated with arachidonic acid and the formed HETEs were assessed, and the basal levels of heart tissue HETEs were also measured by liquid chromatography-tandem mass spectrometry. Results: Our results show significant sexual dimorphism in AAC-induced cardiac hypertrophy. Echocardiography showed more severe hypertrophy in male rats, characterized by an increase in left ventricular mass and wall dimensions. The HW:TL ratio, and the mRNA levels of BNP, SkM α-actin, and β/α-MHC were significantly increased in the hearts of male rats, while only β/α-MHC was increased in female rats. The cardiac mRNA and protein levels of CYP1B1, CYP4A, and CYP4F enzymes were significantly upregulated only in male but not in female rats. The formation rates of all HETEs and the basal 12-HETE level were significantly increased in male rats, while 5-, 9-, and 15-HETE formation were significantly decreased in female rats.

CONCLUSIONS
Male rats developed stronger AAC-induced cardiac hypertrophy compared to female rats, which was associated with a significant increase in cardiac CYP hydroxylases and HETEs. Cardiac CYP enzymes and their metabolites might potentially be involved in the greater risk of cardiovascular diseases like cardiac hypertrophy and heart failure in males.
This work was supported by a grant from the Canadian Institutes of Health Research [CIHR PS 168846] to A.O.S.E-K. S.H.G. is the recipient of Alberta Innovates Graduate Student Scholarship.

Session 1, Recovery of Function oral presentation

A novel small molecule synthesized based on a snail hibernation model, induces hibernation in mouse fibroblasts and perfused hearts

Jiyuan Piao, Yongneng Zhang, Yuan-Yuan Zhao, Patrick Hannington, Amir Tabatabaei-Dakhili, John Ussher, Gopinath Sutendra, Evangelos Michelakis

BACKGROUND
Animals during hibernation suffer no ischemic consequences from their meagre heart/respiration rates, otherwise incompatible with life, but humans lost the ability to hibernate (presumably when their ancestors gained independence from the weather) and are highly vulnerable to ischemia. In a snail hibernation model, we isolated a brain metabolite only present in the plasma and brain of hibernating snails, and we characterized it with NMR and HPLC/MS. We found that it is an activator of PHLPP1, a critical phosphatase in the conserved AMPK/mTOR signalling networks implicated in hibernation and fuel sensing (O2, glucose, amino acids). We synthesized it chemically and named it Snail Neurometabolite Activator of PHLPP1 (SNAP). We hypothesized that SNAP may induce hibernation in snails as well as mouse cells and organs that normally do not exhibit hibernation.

METHODS/RESULTS
SNAP injections in snails induced reversible hibernation indistinguishable from physiologic. SNAP dephosphorylated the PHLPP1 targets AKT, S6K and AMPK in fibroblasts cultured in hypoxic and low-glucose conditions for three days, significantly suppressed O2 consumption, apoptosis, and cell-cycle progression. Upon discontinuation of SNAP and return to normal culture conditions, the SNAP-treated cells had preserved metabolism and re-entered the cell cycle at much higher rates compared to the vehicle, suggesting protection from ischemia and reperfusion (IR) injury and entrance in a reversible hibernation-like state. To study whether such protection from IR injury occurs in an organ with high fuel demand, we gave SNAP in a model of IR using Langendorff-perfused mouse hearts. Compared to the vehicle, SNAP-perfused hearts had significantly higher LV pressure, max and min dp/dt and reentered normal function much earlier at reperfusion.

CONCLUSIONS
SNAP offers protection from IR injury, inducing hibernation in cells and mice hearts, with wide implications for heart attack/stroke, preservation of donated organs for transplantation or even ultra-long space travel.

Poster #17

Intramuscular versus intravenous epinephrine administration in a pediatric porcine model of cardiopulmonary resuscitation

Megan O'Reilly, Janice Tijssen, Tze-Fun Lee, **Marwa Ramsie**, Po-Yin Cheung, Georg M Schmölzer

BACKGROUND
Current American Heart Association Pediatric Life Support guidelines recommend epinephrine administration via intravenous (IV) or intraosseous (IO) route, with endotracheal (ET) administration admissible in the absence of IV/IO access. Establishing IV/IO/ET access might take several minutes and requires specialized equipment or advanced skills, which may not be readily available in all settings. Alternatively, intramuscular (IM) epinephrine could be administered immediately. At present, there is limited data on the use of IM epinephrine in pediatric resuscitation. To compare IM with IV epinephrine in a pediatric porcine model of asphyxia-induced cardiac arrest, and to investigate the effect of muscle perfusion on bioavailability of epinephrine. We hypothesized that in a pediatric animal model of cardiac arrest, IM epinephrine would not be advantageous to IV epinephrine, and the bioavailability of IM epinephrine would be limited due to compromised muscle perfusion.

METHODS/RESULTS
Thirty pediatric piglets (5-10 days old) were anesthetized and randomized to IM or IV epinephrine with bradycardia or asystole cardiac arrest, and control hypoperfused or normoperfused thigh muscle. Heart rate, arterial blood pressure, carotid blood flow, cardiac function, and cerebral oxygenation were continuously recorded throughout the experiment. Time to ROSC and the number of piglets that achieved ROSC were comparable between IM and IV epinephrine groups with either bradycardia and asystole cardiac arrest.

CONCLUSIONS
In a pediatric piglet model of cardiac arrest, administration of IM epinephrine results in similar resuscitative outcomes to IV epinephrine. Effectiveness of IM epinephrine varies depending on the perfusion level of the muscle injected, which could be limited in cases of severe acidosis or during asystole.

Poster #18

Sex Differences in the Murine Response to Lipopolysaccharides: Are Endogenous Ketones Responsible?

Mya Schmidt, Yasser Abuetabh, Heidi Silver, Matthew Martens, Matthieu Zolondek, Jason Dyck

BACKGROUND
Lipopolysaccharide (LPS), a principal component of the outer membrane of Gram-negative bacteria, is frequently used to mimic inflammatory human diseases in preclinical models including sepsis-induced cardiomyopathy. Despite its widespread use in medical research, there are no comprehensive investigations which detail the sex differences that exist in the systemic and cardiac response to LPS. This knowledge is crucial not only for determining whether both sexes are required for studies employing LPS, but also for enhancing our understanding of how males and females differentially manage inflammation. Previously, we have observed that female mice treated with LPS appear healthier and have a less severe plasma cytokine profile than male mice. Additionally, we have observed that female mice have higher fasting levels of the ketone body β-hydroxybutyrate (βHB), which has been shown to exert anti-inflammatory signalling properties through a multitude of signalling pathways including inhibition of the NLR family pyrin domain containing 3 (NLRP3) inflammasome. Therefore, we investigated sex differences in the response to LPS and in ketone metabolism, predicting that females are more protected against LPS-induced multi-organ damage than males due to differences in βHB kinetics.

METHODS/RESULTS
We administered 10 mg/kg of LPS or vehicle (saline) intraperitoneally to wild-type male and female 8-week-old C57BL/6J mice. After 24 hours, we collected their blood and tissues and characterized the expression of genes and proteins involved the inflammatory response and ketone metabolism in the vital organs via PCR and western blot.

We found that LPS-treated females display significantly lower cardiac mRNA expression of the pro-inflammatory cytokines Il-1b and and Tnf-a. Interestingly, we also observed that 24 hours post-administration, LPS-treated female mice have significantly higher circulating levels of βHB. This was further supported by our finding that vehicle-treated females have greater hepatic expression of the ketogenic enzymes HMGCS2 and BDH1 than vehicle-treated males, suggesting a larger capacity to produce ketones in the liver. Surprisingly, we discovered that Il-6 was significantly upregulated in the liver and kidneys of LPS-treated females, but not LPS-treated males. Together, these data suggest that female mice have both a more robust pro-inflammatory and anti-inflammatory response to LPS. In future experiments, we will explore whether βHB is directly involved in mediating the protective effects observed in female mice in response to LPS-induced inflammation.

CONCLUSIONS
Ultimately, this work is part of a larger project that will inform the utility of implementing ketone-centric therapies, such as exogenous ketone supplements, in treating the inflammatory component of cardiovascular diseases.

Poster # 19

Determining the effect and mechanism of action of SARS-CoV-2 spike protein on von Willebrand factor expression and/or release from endothelial cells

Noorossadat Seyyedi, Parnian Alavi, Alexia Maheux, Samar Barazesh, Nadia Jahroudi

BACKGROUND
Von Willebrand factor (VWF) is a highly adhesive multimeric glycoprotein stored in Weibel-Palade bodies (WPBs) of endothelial cells (ECs) and α-granules of megakaryocytes. VWF multimers released from ECs through basal or regulated secretion may remain bound to cell membrane or enter the circulation. VWF mediates platelet adhesion to endothelial/subendothelial surfaces, and promotes platelet aggregate formation, thus maintaining hemostasis but could also contribute to thrombogenicity. In addition to injury, various stimuli including bacterial and viral infections are associated with increased VWF levels. COVID-19 is an infection caused by a virus known as severe acute respiratory syndrome coronavirus 2 (SARS-CoV-2). Those severe and critically ill COVID-19 patients with significant thrombotic complications were shown to have highly elevated levels of VWF. Although the increase in VWF levels may result from a rise in inflammatory response to SARS-CoV-2, we hypothesized that this virus may also directly induce VWF upregulation and/or release from ECs. Since the receptor for SARS-CoV-2 spike protein, angiotensin-converting enzyme 2 (ACE2), is present on EC surfaces; we hypothesized that spike protein engagement of the ACE2 receptor may lead to VWF transcriptional upregulation and/or release from WPBs, and consequently contribute to increased platelet aggregate formation and thrombogenicity.

METHODS/RESULTS
Human umbilical vein endothelial cells (HUVECs), human brain microvascular endothelial cells (Brain MVECs), and human lung microvascular endothelial cells (Lung MVECs) were treated with SARS-CoV-2 spike protein. Cell lysate and culture media were collected at various time points after treatment. Exposure to SARS-CoV-2 spike protein resulted in a significant increase in released VWF in culture media of Lung MVECs and HUVECs, but not Brain MVECs within five minutes. Analyses of VWF mRNA levels revealed a significant increase specifically in Lung MVECs after 48-72 hours of treatment. VWF multimer analysis of culture media and cell lysate of HUVECs and Lung MVECs demonstrated an increase in the most biologically active high molecular weight (HMW) VWF multimers after exposure to spike protein. Immunofluorescence staining using an anti-ACE2 antibody confirmed the presence of this protein in all three endothelial cell types.

CONCLUSIONS
Our results demonstrated that SARS-CoV-2 spike protein directly induces VWF transcriptional upregulation, leading to HMW VWF multimers storage and release from ECs in a highly organ-specific manner, specifically in Lung MVECs. Elevated VWF secretion was detected in HUVECs and Lung MVECs, but VWF mRNA upregulation was observed only in Lung MVECs. Brain MVECs did not respond to spike protein exposure at either level.

Session 4, 3MT-style presentation

New and persistent psychoactive medication use in intensive care survivors with COVID-19

Andrea C Shysh, Finlay A McAlister, Luan Manh Chu, Jason Weatherald, Sean M Bagshaw, Ken Kuljit S Parhar, Fernando G Zampieri, Jacob C Jentzer, Erik Youngson, Sameer S Kadri, Padma Kaul, Sean van Diepen

BACKGROUND
INTRODUCTION: COVID-19 intensive care unit (ICU) survivors may have higher rates of post-intensive care syndrome. Our objective was to determine the frequency and predictors of new psychoactive medication prescriptions at hospital discharge in COVID-19 ICU survivors and to describe the associated one-year clinical outcomes.

METHODS/RESULTS
METHODS: This is a retrospective, multi-center, population-based cohort study using linked provincial health datasets to define the cohort, comorbidities, ICU interventions, laboratory values, and medication dispensations. Adults admitted to an ICU with a diagnosis of COVID-19 and survived to hospital discharge between January 1, 2021 and July 31, 2022 were included. Adults with a psychoactive prescription filled in the 6 months prior to index hospitalization were excluded. New psychoactive medication recipients were identified at discharge as well as persistent recipients after one year. Multivariable regression was used to identify factors associated with new psychoactive use and the association with one-year all-cause mortality, hospital readmission, and emergency room (ER) visits.
RESULTS: Among 1,486 psychoactive-naïve adults (mean 56 years, 67.5% male) who survived an ICU stay with COVID-19 (mean ICU length of stay [LOS] 6.6 days, mean hospital LOS 17.1 days), 261 (17.6%) were prescribed psychoactive medications at hospital discharge. Common prescriptions included benzodiazepines (41%), opioids (28.3%), anti-psychotics (20.3%), and selective serotonin reuptake inhibitors (15.0%). At one year, 135 (51.7% of new recipients) had persistent medication dispensations. Independent predictors of new psychoactive prescriptions included pre-admission diagnosis of anxiety (adjusted Odds Ratio [aOR] 3.40; 95% CI 1.62-7.12), rural residence (aOR 1.48; 95% CI 1.06-2.05), and hospital LOS (aOR 1.01; 95% CI 1.00-1.01) but there was no significant association with ICU therapies or acuity scores. Patients with new discharge prescriptions had higher one-year all-cause mortality (10.3% vs. 5.4%, aOR 2.26, 95% CI 1.01-5.07) and ER visits (58.2% vs. 41.8%, aOR 1.66, 95% CI 1.14-2.41).

CONCLUSIONS
CONCLUSION: New psychoactive medications were common in COVID-19 ICU survivors and approximately half of patients were still receiving medications one-year later. Our finding that new post-discharge psychoactive medications were associated with a higher risk of mortality and ER visitation suggests the need to reassess medication appropriateness at the time of discharge and during follow-up.

Figure 1. One-year outcomes after index hospital discharge in COVID-19 ICU survivors, stratified by new psychoactive use at the time of index hospital discharge.

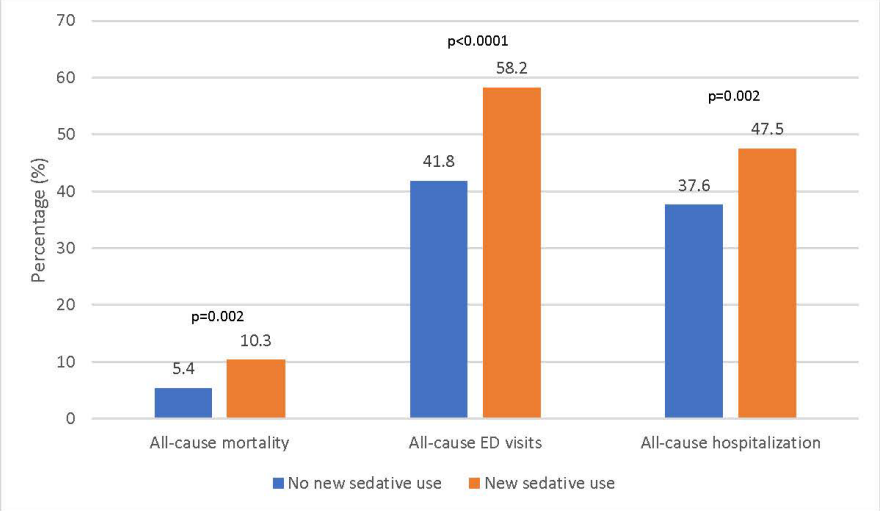

Abbreviations: ICU, intensive care unit; ED, emergency department.

Session 2, Vascular Function oral presentation

Prevalence, Burden, and Manifestation of Atrial Fibrillation: A large-scale analysis of long-term cardiac monitoring exams.

Sophie Sigfstead, Jonathan Neault, Pierre Fecteau, Isabelle Nault, David Gladstone, Riyaz Kaba, Christopher C. Cheung

BACKGROUND
Atrial Fibrillation (AF) is the most prevalent cardiac arrhythmia (occurring in approximately 10% of the population over 65 years of age) and represents significant morbidity and mortality as a leading cause of stroke and heart failure. However, due to its paroxysmal nature, and consequent underdiagnosis, AF prevalence is likely underestimated. Furthermore, due to limited availability of long-term cardiac monitoring data, little information exists regarding the nature of AF episodes within different disease subtypes (i.e. paroxysmal vs. persistent AF). To address this gap, we evaluated monitoring data from patients undergoing cardiac patch monitor from May 2017 to July 2023.

METHODS/RESULTS
Patch monitors reports performed during the study period (May 2017-July 2023) were provided in a fully anonymized manner for analysis (iCentia CardioSTAT™, Quebec City, QC). Patients underwent monitoring for varying durations, from 24-hours up to 14 days. Population demographics and summary statistics were calculated, stratified across AF subtype (i.e. low-burden AF defined as AF burden ≤10%; high-burden AF defined as AF burden ≥95%). AF burden was calculated by the time in AF divided by the total monitoring duration.

Patch monitor records from 130,042 patients (142,346 recordings) were analyzed. Patients had a mean age of 61.6±18.8 years with 50.5% female (43.7% male, 5.8% unspecified). On average, patients performed 1.09±0.36 patch monitors during the study period, lasting a median of 168 hours (range: 24-336 hours). The AF prevalence was 11.13%, with a mean AF burden of 58.5% among those with AF detected (Figure 1).

Among those with AF detected, low-burden and high-burden AF was detected in 5013 patients (31.6%) and 8358 patients (52.7%), respectively. There were significant differences in episode characteristics and patient-reported symptoms observed between these two groups (Table 1). Low AF patients had significantly higher mean, maximum and minimum heart rate during episodes and were more symptomatic during monitoring ($p<0.01$ for all).

CONCLUSIONS
While this analysis was conducted within a selected population undergoing cardiac monitoring, the measured incidence of AF highlights the commonality of the condition. The observed differences between low-burden and high-burden AF patients indicates that there exist significant differences in arrhythmia characteristics, with patients with low-burden AF having AF at faster heart rates compared to high-burden AF patients. Patients with low-burden AF more frequently reported symptoms during their monitoring period, compared to high-burden AF patients. These findings provide important insights into the detection and management of AF, with differences in arrhythmia characteristics and symptomatology based on arrhythmia subtype.

Figure 1: Histogram of AF Burden in those with AF Detected by Patch Monitor

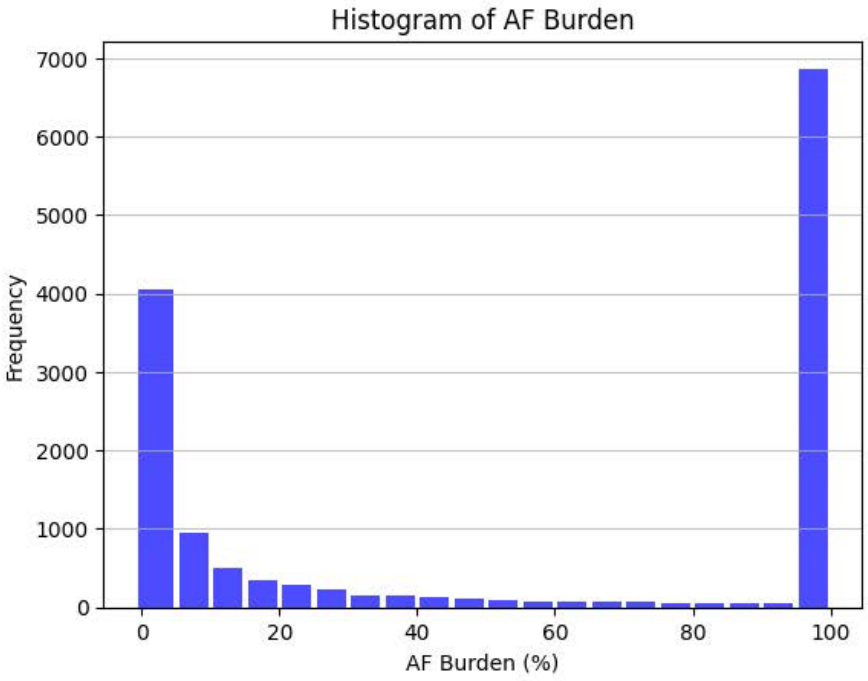

Table 1: AF Episode Characteristics and Symptoms, Stratified by Low-Burden and High-Burden AF

	Low-Burden AF (n = 5013)	High-Burden AF (n = 8358)	P-value
Episode Characteristics:			
Mean Number of AF episodes per 24 hours of monitoring	2.53±10.3	0.36±1.4	**<0.001**
Mean HR during AF episode (bpm)	110.1±26.1	78.0±16.0	**<0.001**
Maximum HR during AF episode (bpm)	160.4±35.0	147.0±31.7	**<0.001**
Minimum HR during AF episode (bpm)	73.7±22.8	45.7±10.9	**<0.001**
Symptoms experienced during monitoring (%):			
Palpitations	32.6	25.3	**<0.001**
Pain	20.6	17.1	**<0.001**
Dizziness	22.5	19.7	**<0.001**
Shortness of Breath	25.0	27.5	**<0.01**
Other Symptoms	26.0	22.1	**<0.001**
No Symptoms	3.1	3.2	0.75

Poster #20

Role of Activin A in Cancer-Mediated Cachexia

Amro M. Soliman, Kasia Dzierlega, Xavier Clemente-Casares

BACKGROUND
Cachexia stands as a significant contributor to cancer-related death. Cachectic patients suffer from wasting of cardiac and skeletal muscles, along with adipose tissue. While various cellular and soluble agents have been suggested as contributors to cachexia, the precise mechanisms responsible for the muscle-wasting aspect remain inadequately understood. We previously highlighted polymorphonuclear myeloid-derived suppressor cells (PMN-MDSCs) to be critical for cachexia development in murine cancer models. These cells were found to be a major source of Activin A, contributing to cachexia muscle loss.

METHODS/RESULTS
To induce cachexia, mice were injected with a murine Lewis Lung Carcinoma cell line and euthanized after 2 weeks to assess muscle mass along with flow cytometric evaluation of PMN-MDSC. To elucidate the mechanistic contribution of Activin A-producing PMN-MDSCs to cachexia, we utilized a myeloid/PMN-MDSC-specific Cre-recombinase mouse model.
Myeloid/PMN-MDSC-specific deletion of Activin A gene protected against cardiac and skeletal muscle wasting; however, it did not impact the expansion of these cells to muscle tissues. Western blot analysis confirmed Activin A to activate a downstream signalling pathway that involves phosphorylation of Smad2/3. RNA seq analysis of muscle tissue in tumor-bearing mice revealed an upregulation of mitophagy and protein degradation markers as well as an inhibition of oxidative phosphorylation. Interestingly, knocking out Activin A gene in PMN-MDSCs reversed these effects and guarded against muscle loss under tumor burden.

CONCLUSIONS
Collectively, we demonstrate that PMN-MDSCs produce activin A that induces cachectic muscle wasting via triggering pathways facilitating contractile protein degradation and altering energy production. Targeting this immune/hormonal axis can open the door toward the development of novel therapeutic applications for cancer-associated cachexia.
Funding: Canadian Institutes of Health Research grant# RES0052619

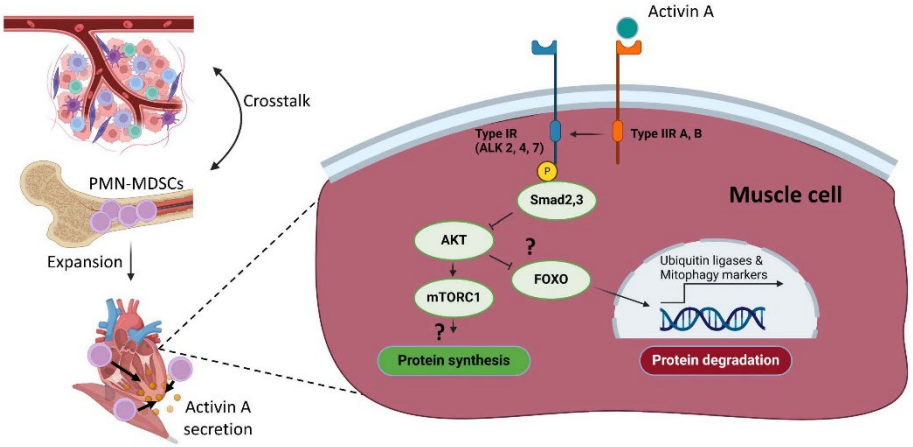

Session 1, Recovery of Function oral presentation

Increasing ketone supply to the heart does not exert functional benefits in mice with heart failure with preserved ejection fraction (HFpEF)

Qiuyu Sun, Cory S. Wagg, Nathan Wong, Liye Fang, John M. Seubert, Timo D. Müller, Gary D. Lopaschuk

BACKGROUND
Heart failure with preserved ejection fraction (HFpEF) is a heterogenous and complex disease associated with many risk factors. Dramatic alterations of cardiac energy metabolism occur in HFpEF mice hearts, including a decrease in glucose oxidation and an increase in fatty acid oxidation. However, although oxidation of ketones is an important source of ATP it remains unclear how the heart oxidizes ketones in HFpEF. It is also unclear whether elevating ketone supply to the heart can improve cardiac energetics and/or provide functional benefit for the hearts in HFpEF. The goal of the study is to investigate the physiological and molecular effects of increasing ketone supply to the heart via ketone ester supplementation or SGLT2 inhibitor treatment.

METHODS/RESULTS
13-month-old C57BL/6N female mice were administered a 60% high fat diet and L-NAME (0.5g/L/day in the drinking water) to induce HFpEF. In parallel, two other groups of mice were maintained on the HFpEF protocol while also receiving either a ketone ester supplement (1-3 butanediol 1g/kg/day) or SGLT2 inhibitor (empagliflozin 10mg/kg/day) for 6 weeks. Cardiac function was assessed with transthoracic echocardiography prior to isolated working heart perfusions. Hearts were perfused with 5 mM glucose, 0.8 mM palmitate, 100 µU/ml insulin, at both low (0.6 mM) and high (1 mM) concentration of [3-14C] β-hydroxybutyrate to quantitatively assess heart ketone oxidation rates.

Mice receiving HFpEF protocol showed accelerated weight gain, glucose intolerance, and elevated blood pressure. Cardiac %EF was preserved in HFpEF mice, but a worsening of diastolic function was seen. In isolated working control hearts, ketone oxidation rates significantly increased in response to higher concentration of β-hydroxybutyrate in the perfusate (0.6 mM vs 1mM) (from 861 ± 63 to 1377 ± 94 nmol.g dry wt-1.min-1). However, in HFpEF hearts, the increase in ketone oxidation rates was significantly decreased (from 707 ± 65 to 881 ± 115 nmol.g dry wt-1.min-1). This was associated with a decreased expression of the ketone oxidative enzyme succinyl-CoA:3-oxoacid CoA transferase (SCOT) in HFpEF hearts. While both ketone ester supplementation and SGLT2i treatment restored ketone oxidation rates in HFpEF hearts, this was not associated with an increased expression of SCOT, or with an improvement in cardiac function.

CONCLUSIONS
Cardiac ketone oxidation is impaired in HFpEF. While increasing ketone supply to the heart restores cardiac ketone oxidation rates, this is not associated with improvements in cardiac function in HFpEF mice.

Poster #21

Pediatric obesity and cardiometabolic health: the importance of healthy lifestyle behaviors

Flavio T. Vieira, Camila E. Orsso, Nandini Basuray, Reena L. Duke, Mohammadreza Pakseresht, Daniela A. Rubin, Faria Ajamian, Geoff D. C. Ball, Catherine J. Field, Carla M. Prado, Andrea M. Haqq

BACKGROUND
Although adolescents with obesity have an increased risk of cardiometabolic disease, a subset maintains a healthy cardiometabolic profile. Unhealthy lifestyle behaviors may determine cardiometabolic risk. We aimed to characterize lifestyle behaviors of adolescents with obesity, compare differences between metabolically healthy (MHO) and unhealthy obesity (MUO), and assess associations between lifestyle behaviors and cardiometabolic profiles.

METHODS/RESULTS
Participants aged 10-18 years with BMI≥95th percentile were included. Dietary intake was estimated from 3-day food records and diet quality using the Healthy Eating Index-Canadian Adaptation. Physical activity (7-day accelerometry), body composition (air-displacement plethysmography), anthropometrics (BMI, waist and hip circumferences), blood markers (glucose control, lipid panel, inflammation markers), and blood pressure (triplicate) were objectively measured. Delay discounting was evaluated as a measure of choice impulsivity using a 5-item adjusting task. MUO was defined as high triglycerides, blood pressure, glucose, or low high-density lipoprotein. Regression analyses were performed between lifestyle behaviors (dietary intake, diet quality, physical activity, and choice impulsivity) and cardiometabolic markers and adjusted by sexual maturation (pre-early versus mid-late).

Thirty-nine participants (BMI z-score 2.8 [2.5-3.5], age 12.5 [10.9-13.5] years, 56.4% female) were included. A high proportion of participants failed to meet lifestyle recommendations, particularly for diet quality (94.7%, n=36), fiber (94.7%, n=36), and physical activity (90.9%, n=30). No differences in lifestyle behaviors were found between MUO (59.0%, n=22) versus MHO (41.0%, n=16). Protein intake was negatively associated with BMI and waist circumference z-scores, fat mass index, insulin resistance, low-density lipoprotein, and C-reactive protein; while higher diet quality was associated with lower C-reactive protein. A higher proportion of carbohydrates in the diet relative to total energy intake was associated with a less favorable lipid profile (total cholesterol and low-density lipoprotein). In turn, a healthier carbohydrate intake (whole grain and total grain scores) was associated with a more favorable cardiometabolic profile (lower BMI z-score and glucose levels, respectively). Higher light physical activity levels were associated with lower total cholesterol and triglycerides. Greater choice impulsivity was associated with higher total cholesterol, low-density lipoprotein, and triglyceride concentrations.

CONCLUSIONS
Adolescents with either metabolically healthy or unhealthy obesity showed low adherence to recommendations for dietary intake (especially fiber), diet quality (healthy eating index), and physical activity. No differences in lifestyle behaviors were found between MUO and MHO. Protein intake, diet quality (overall and carbohydrate), and physical activity were associated with a healthier cardiometabolic profile.

Table 1. Demographic, health status, lifestyle behaviors, and cardiometabolic parameters of adolescents with obesity, overall sample and stratified by metabolically unhealthy (MUO) and healthy obesity (MHO)

Variables	n	Overall sample	n	Adolescents with MUO	n	Adolescents with MHO	P-value
Age (years)	39	12.5 (10.9-13.5)	23	12.8 (11.2-15.3)	16	12.2 (10.9-13.3)	0.422
Sex (female, %)	22	56.4	13	56.5	9	56.3	0.987
Puberty Stage							
Pre-early puberty (%)	16	41.0	8	34.8	8	50.0	0.342
Mid-late puberty (%)	23	59.0	15	65.2	8	50.0	
Race/ethnicity							
White (%)	21	55.3	14	60.9	7	46.7	0.389
Indigenous (%)	9	23.7	5	21.7	4	26.7	
Others (%)	8	21.1	4	17.4	4	26.7	
Health conditions							
Insulin Resistance (%)	24	63.2	15	68.2	9	56.3	0.452
Dyslipidemia (%)	18	47.4	17	77.3	1	6.3	**<0.001**
Hypertension (%)	11	28.2	10	43.5	1	6.3	**0.014**
Metabolic syndrome (%)	5	14.7	5	25.0	0	0	0.063
Dietary intake							
Total energy intake (kcal/day)	38	1870 (1560-2140)	22	1790 (1430-2075)	16	1920 (1754-2410)	0.149
Total energy intake (kcal/body weight)	38	24 (17-29)	22	22 (14-29)	16	25 (22-33)	0.144
Protein (%)	38	17.2 (15.6-19.3)	22	17.1 (15.3-19.2)	16	17.8 (14.8-19.9)	0.804
Protein (g/1,000 kcal)	38	43.3 (40.1-49.1)	22	43.2 (40.1-48.2)	16	44.6 (39.9-50.6)	0.693
Protein (g/body weight)	38	1.0 (0.7-1.3)	22	0.9 (0.6-1.2)	16	1.2 (0.8-1.5)	0.095
Protein below EAR (%)	38	28.9	22	36.4	16	18.8	0.296
Fat (%)	38	33.7 (30.3-37.9)	22	33.1 (29.7-35.3)	16	35.7 (30.7-39.6)	0.145
Fat outside AMDR (%)[a]	38	47.4	22	36.4	16	62.5	0.111
Fat (g/1,000 kcal)	38	37.7 (35.1-42.3)	22	37.1 (35.1-39.9)	16	40.1 (35.6-44.5)	0.145
Saturated fat (%)	38	10.6 (6.5-13.5)	22	10.4 (8.2-13.6)	16	11.5 (0.1-12.7)	0.715
Monounsaturated fat (%)	38	10.7 (4.8-12.5)	22	10.7 (8.1-12.3)	16	10.9 (0.1-14.5)	0.804
Polyunsaturated fat (%)	38	4.6 (1.9-6.8)	22	5.1 (3.7-7.1)	16	4.4 (0.1-6.4)	0.212
Trans fat (g)	38	1.0 (0.4-2.5)	22	0.7 (0.4-2.3)	16	1.8 (0.7-2.7)	0.298
Carbohydrate (%)	38	49.2 (44.2-52.8)	22	51.0 (45.4-53.5)	16	45.3 (40.7-52.7)	0.234
Carbohydrate outside AMDR (%)[b]	38	39.5	22	27.3	16	56.3	0.071
Carbohydrate (g/1,000 kcal)	38	125.9 (112.5-134.9)	22	129.7 (118.1-136.3)	16	115.1 (103.9-133)	0.201
Fiber total (g)	38	16.7 (12.6-20.5)	22	15.4 (10.7-23.5)	16	17.5 (14.7-19.8)	0.672
Fiber (g/1,000 kcal)	38	8.4 (7.5-11.2)	22	8.6 (7.5-11.5)	16	8.4 (7.7-9.2)	0.458
Fiber below AI (%)	38	94.7	22	95.5	16	93.8	1.0
Healthy Eating Index: 0 to 100 points							
Healthy Eating Index Total score	38	63.1 (53.7-69.4)	22	64.3 (53.7-72.5)	16	61.3 (53.9-68.5)	0.625
Healthy Eating Index <80 (n, %)	38	94.7	22	95.4	16	93.8	1.0
Adequacy components: 0 to 60 points							
Total vegetables and fruit score	38	6.9 (4.8-10.0)	22	6.6 (4.1-10.0)	16	7.4 (5.9-10.0)	0.529
Whole fruit score	38	2.9 (1.7-4.1)	22	2.8 (1.7-4.3)	16	3.0 (1.8-4.0)	0.739
Dark green and orange vegetables and legumes score	38	1.3 (0.2-3.6)	22	1.4 (0-3.6)	16	1.3 (0.3-3.9)	0.651
Total grain products score	38	3.7 (2.7-5.0)	22	3.7 (2.6-5.0)	16	3.8 (2.6-5.0)	0.759
Whole grains score	38	2.9 (0.6-3.8)	22	2.8 (0.6-4.3)	16	3.0 (0.2-3.4)	0.895
Milk and alternatives score	38	4.7 (2.8-6.4)	22	4.7 (3.0-7.7)	16	4.6 (2.0-5.6)	0.344
Meat and alternatives score	38	10.0 (9.9-10.0)	22	10.0 (7.7-10.0)	16	10.0 (10.0-10.0)	0.298
Unsaturated fats score	38	9.9 (8.6-10.0)	22	9.0 (8.2-10.0)	16	10.0 (9.0-10.0)	0.212
Moderation components: 0 to 40 points							
Saturated fats score	38	6.2 (1.6-8.5)	22	7.3 (2.2-8.8)	16	4.5 (0.2-7.9)	0.137
Sodium score	38	5.8 (2.4-8.2)	22	6.0 (4.1-8.7)	16	5.1 (0.3-6.8)	0.087
Other food score	38	12.1 (7.3-16.0	22	13.8 (6.3-16.0)	16	11.4 (7.9-15.7)	0.781
Physical Activity levels							
Sedentary time (min/day)	33	610 (533-673)	22	607 (540-692)	11	610 (495-637)	0.387
Sedentary (% of the day)	33	74.7 (70.1-82.7)	22	75.6 (70.1-83.6)	11	74.7 (70.0-80.6)	0.355
Light physical activity (min/day)	33	159 (113-186)	22	142 (96-182)	11	161 (144-189)	0.268
Light physical activity (% of the day)	33	19.6 (14.4-23.5)	22	19.1 (12.9-23.8)	11	20.5 (15.7-24.7)	0.281
Moderate-to-vigorous physical activity (min/day)	33	40 (29-50)	22	40 (27-55)	11	40 (33-44)	0.895

Moderate-to-vigorous physical activity (% of the day)	33	4.8 (3.6-6.6)	22	5.1 (3.4-6.6)	11	4.8 (3.7-5.6)	0.955
Moderate-to-vigorous physical activity <60 min/day (%)	33	90.9	22	90.9	11	90.9	1.0
Delay discounting decision-making							
Effective Delay 50%	39	210.9 (105.4-2310.0)	23	210.9 (105.4-2310.0)	16	223.7 (74.6-3000.5)	0.810
Effective Delay (k)	39	0.0067 (0.0011-0.0134)	23	0.0047 (0.0019-0.0095)	16	0.0081 (0.0009-0.0095)	0.582
Cardiometabolic parameters							
Body mass index z-score	39	2.8 (2.5-3.5)	23	3 (2.5-3.6)	16	2.8 (2.5-3.3)	0.384
Waist circumference z-score	34	1.7 (1.4-1.9)	20	1.7 (1.6-2.1)	14	1.6 (1.3-1.7)	0.319
Waist-to-hip ratio	34	0.88 (0.84-0.93)	20	0.89 (0.85-0.93)	14	0.87 (0.83-0.94)	0.793
Waist-to-height ratio	34	0.57 (0.53-0.62)	20	0.60 (0.54-0.63)	14	0.56 (0.51-0.58)	0.086
Fat mass (%)	22 17	40.3 (37.1-43.9) F 42.5 (36.9-46.7) M	13 10	42.3 (38.7-45.3) F 43.8 (40.3-48.5) M	9 7	38.9 (37.1-40.0) F 41.6 (35.8-45.5) M	0.190
Fat mass index (kg/m^2)	22 17	11.06 (9.90-13.91) F 13.57 (10.07-18.87) M	13 10	12.1 (10.7-14.5) F 14.5 (11.3-19.3) M	9 7	10.2 (10.1-11.0) F 13.6 (9.3-14.2) M	0.151
Fat-free mass (kg)	22 17	43.4 (36.7-52.4) F 52.3 (40.0-64.1) M	13 10	45.5 (37.2-53.1) F 58.1 (43.0-63.3) M	9 7	42.8 (41.6-45.9) F 48.0 (41.4-64.9) M	0.582
Fat-free mass index (kg/m^2)	22 17	17.34 (15.42-19.72) F 19.06 (16.71-20.86) M	13 10	17.6 (15.4-19.8) F 19.2 (17.1-20.6) M	9 7	17.2 (17.0-18.4) F 19.1 (17.0-21.3) M	0.641
Glucose (mg/dL)	38	90.0 (86.4-91.8)	22	90 (86.4-90)	16	88.2 (86.4-91.8)	1.000
Insulin (pmol/L)	39	113.2 (82.6-138.2)	23	118.1 (96.9-152.1)	16	96.5 (70.4-125.5)	0.130
HOMA-IR	38	3.61 (2.56-4.37)	22	3.71 (3.11-4.97)	16	3.21 (2.22-4.05)	0.181
Total cholesterol (mg/dL)	38	146.2 (128.8-169.8)	22	150.8 (135.3-170.1)	16	139.2 (85.1-158.5)	0.122
HDL-c (mg/dL)	39	41.0 (38.7-47.2)	23	39.1 (34-44.1)	16	44.1 (41.9-48.7)	**0.004**
LDL-c (mg/dL)	39	85.1 (71.7-98.0)	23	90.1 (79.1-101.3)	16	77.7 (66.4-94.4)	0.146
Triglycerides (mg/dL)	39	93.0 (79.3-116.9)	23	103.6 (84.6-132.9)	16	81.5 (74.6-95)	**0.014**
C-reactive protein (mg/dL)	36	1.7 (0.73-5.0)	20	2 (0.9-6.3)	16	1.3 (0.7-2.2)	0.268
Interleukin-6 (pg/mL)	28	9.4 (6.8-25.1)	19	9.6 (6.8-28.1)	9	9.3 (6.1-21.7)	0.731
TNF-α (pg/mL)	28	17.7 (1.6-42.4)	19	18.1 (3.8-46.7)	9	10.6 (1-36.9)	0.655
Systolic blood pressure percentile	39	83 (65-95)	23	89 (72-99)	16	78 (61-90)	0.055
Diastolic blood percentile	39	74 (41-86)	23	78 (53-92)	16	57 (36-76)	**0.031**

Data is presented as median (interquartile range) or percentage (%)

AI: adequate intake fiber, males 9-13y 31g, 14-18y 38g, females 9-18y 26g; AMDR: acceptable macronutrient distribution range fat 25-35%, carbohydrate 45-65%; EAR: estimated average requirement for protein males 9-13y 0.76g/kg, 14-18y 0.73g/kg; females 9-13y 0.76g/kg, 14-18y 0.71g/kg; F: females; HDL-c: high-density lipoprotein cholesterol; HOMA-IR: homeostatic model assessment for insulin resistance; IQR: interquartile range; LDL-c: low-density lipoprotein cholesterol; M: males; TNF- α: tumor necrosis factor-alpha

Significant differences between MUO and MHO are highlighted in bold, p <0.05.

[a] Majority of non-adherence (15/18) was above fat recommendation range.

[b] Majority of non-adherence (12/15) was below carbohydrate recommendation range.

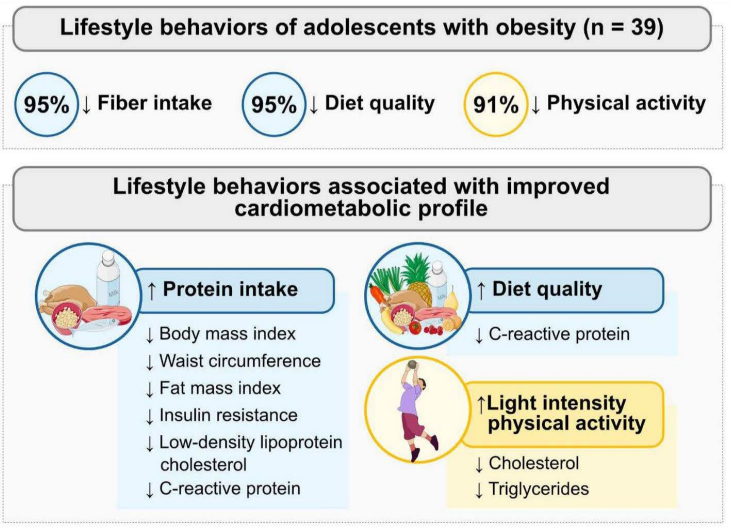

Figure 1. Graphical summary

Session 4, 3MT-style presentation

Tumour Secreted Inosine and Hypoxanthine Promote RBFOX1 Degradation, Cardiomyocyte Dedifferentiation and Susceptibility to Cardiotoxicity

Saymon Tejay, Maria Areli Lorenzana-Carillo, Seyed Amirhossein Tabatabaei-Dakhili, Yuan Yuan Zhao, Farah Eaton, Michelle Mendiola Pla, Dawn E Bowles, Ian D Patterson, Edith Pituskin, John R Ussher, Evangelos Michelakis and Gopinath Sutendra

BACKGROUND
It is well established that cancer cells can secrete numerous signalling factors that affect distant normal tissues such as skeletal muscle or adipose tissue break down by tumour necrosis factor (TNFa) and lipid mobilizing factor (LMF) respectively. What remains unclear is if tumour secreted factors (TSFs) can initiate a signalling cascade in cardiomyocytes to render these cells more susceptible to cell death and cardiotoxicity after DNA damaging chemotherapy treatment, a common adverse side effect.

METHODS/RESULTS
Clinically relevant tumour xenotransplant mice were used to identify TSFs in the serum and their effect on the myocardium. Serum and tumour biopsies were collected from breast cancer patients prior to treatment and development of cardiotoxicity. We generated cardiomyocyte-specific RBFOX1-deficient and gastric tissue specific ZNF281 overexpressing mice and assessed myocardial signalling and heart function (via echocardiography) prior to and after chemotherapy (anthracycline) treatment. Human chemotherapy induced cardiotoxicity myocardial biopsies were used to translate mechanistic findings. A ZNF281 inhibitor was developed to inhibit TSF production and prevent cardiotoxicity after chemotherapy treatment in tumor xenotransplant mice.

We found that tumour secreted inosine and hypoxanthine were significantly elevated in the serum of lung cancer mice and breast cancer patients that developed cardiotoxicity. Mechanistically, we found that the metastatic transcription factor ZNF281 increases tumour secreted inosine and hypoxanthine that can bind and activate the A2A receptor on cardiomyocytes, activating CAMKIIδ, which phosphorylates the postnatal mRNA splicing factor RBFOX1 on threonine-197, resulting in its caspase-dependent degradation. Loss of RBFOX1 initiates epigenetic remodeling, cardiomyocyte dedifferentiation and loss of a post-natal mitochondrial splice variant of GRB7 thus promoting the formation of a functional mitochondrial permeability transition pore (mPTP). Activation of the mPTP allows for the release of the pro-apoptotic factor, cytochrome C, into the cytoplasm which signals cell death in proliferative cells but not terminally differentiated cardiomyocytes as they lack the second substrate, APAF1, for apoptosome formation. The presence of cytoplasmic cytochrome C increases susceptibility to apoptosis and cardiotoxicity as several chemotherapies can induce APAF1. RBFOX1- deficient and ZNF281 OE male and female mice develop significant cardiotoxicity when treated with low dose doxorubicin (commonly used DNA intercalating chemotherapy). Tumor ZNF281 inhibition decreased serum inosine levels and preserved cardiac function in lung cancer mice after doxorubicin treatment. RBFOX1 loss correlated with cell death markers (APAF1, P53, cleaved caspase 9) in anthracycline-mediated cardiotoxicity patients.

CONCLUSIONS

This work identified a potential biomarker (i.e. inosine/ hypoxanthine), mechanism for susceptibility to cardiotoxic anti-cancer drugs and a therapeutic target (ZNF281) to prevent cardiotoxicity.

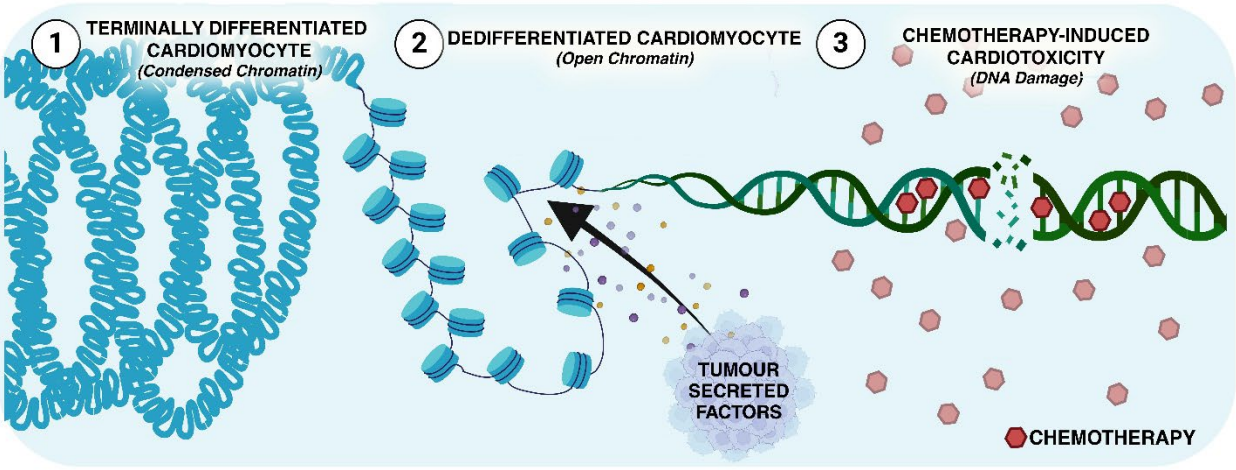

Poster #22

3D-3D rigid registration of echocardiographic images with significant overlap using particle filter

Thanuja Uruththirakodeeswaran, Michelle Noga, Lawrence H Le, Pierre Boulanger, Harald Becher, Kumaradevan Punithakumar

BACKGROUND
The precise alignment of 3D echocardiographic images taken from different views has been shown to enhance the image quality and increase the field of view. This study proposes a novel sequential Monte Carlo (SMC) algorithm for 3D-3D rigid registration of transthoracic echocardiographic images with significant overlap.

METHODS/RESULTS
We used a SMC algorithm for 3D-3D rigid registration of echocardiographic images that is robust to the noise present in ultrasound images. The proposed algorithm estimates the translational and rotational components of the rigid registration through an iterative process. The method requires an initial approximation of the rotation and translation limits that depend on the dimension of the image and the initial overlap between images. The registration is performed in two ways that the same transform approach applies the transform computed for the end diastolic frame to all frames of the cardiac cycle, whereas the unique transform approach registers each frame independently. The proposed SMC and exhaustive search (baseline) algorithms were evaluated for 3D volumes of a cardiac cycle using the proposed approaches. The method was evaluated in 3D echocardiographic volumes recorded from 3 patients who participated in a research study conducted at the Mazankowski Alberta Heart Institute. The experimental evaluations demonstrate that the same transform approach yielded a Dice score value of 0.743 ± 0.041 measured in terms of Dice score for the left ventricle, and required less computational time than the unique transform approach or exhaustive search. The SMC performs better than the exhaustive search at 0.05 significance level. The accuracy was improved further using the simple elastix deformable registration algorithm to fix misalignments due to deformations and yielded an overall Dice score value of 0.779 ± 0.042.

CONCLUSIONS
The SMC based approaches perform well compared to the exhaustive search in terms of accuracy and computational time. Even though the same and unique transform based methods offer similar overall registration accuracies, the same transform approach requires significantly less computational time to compute the final results.

Table 1: The rigid registration results for image pairs using mean Dice score (DSC) for minimum, maximum, and percentile values are shown for unique (u) vs same (s) transform approaches for particle filter (PF) and exhaustive search (ES) methods. The elastix registration is performed on PF_s results.

Method	Minimum	Q1 (25%)	Q2 (50%)	Q3 (75%)	Maximum
Initial DSC	0.425	0.606	0.669	0.822	0.845
PF_u	0.537	0.698	0.743	0.828	0.890
ES_u	0.593	0.617	0.652	0.819	0.890
PF_s	0.526	0.678	0.763	0.834	0.897
ES_s	0.547	0.641	0.663	0.699	0.823
PF_s + Elastix	0.657	0.696	0.778	0.873	0.896

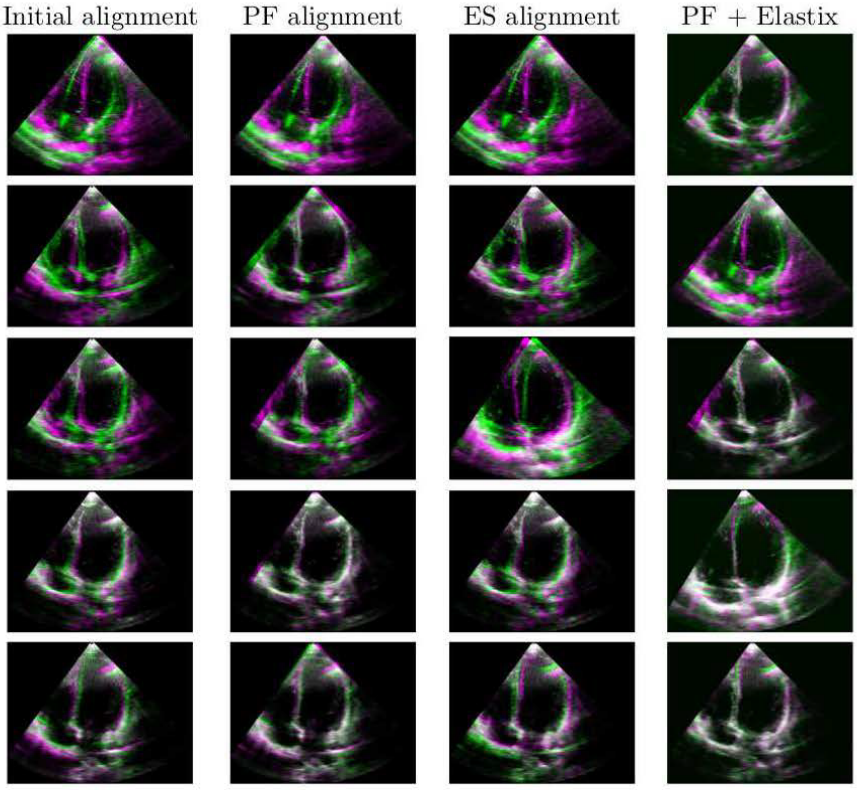

Figure 1: The rigid (PF, ES) and non-rigid (Elastix) registration results of the first frame of image pairs for min (0%), Q1 (25%), Q2 (50%), Q3 (75%), and max(100%) DSC values of coronal view, respectively. The source and target images are shown in green and purple colors.

Session 1, Recovery of Function oral presentation

Investigating elamipretide as a potential therapeutic for sepsis-induced cardiac dysfunction

Jennie Vu, Claudia Holody, Si Ning Liu, Ibrahim Khodabocus, Kimberly Macala, Stephane Bourque

BACKGROUND
Sepsis is an often fatal condition characterized by a dysregulated host immune response to infection leading to organ dysfunction. Cardiovascular dysfunction precedes the development of multi-organ failure and mortality in sepsis. The septic heart is characterized by attenuated biventricular systolic and diastolic function resulting in a blunted ejection fraction and decreased ventricular compliance; this may be due to inflammation-induced cardiomyocyte injury, and metabolic aberrations involving mitochondrial dysfunction. Mitochondrial perturbations can cause cardiomyocyte damage and energetic failure, suppressing myocardial function. Sepsis survivors face long-term cardiovascular impairments and are at an increased risk of adverse cardiovascular events. There are currently no targeted interventions to address acute or persistent sepsis-induced cardiac dysfunction. Elamipretide is a peptide that facilitates the assembly of electron transport chain supercomplexes, promoting efficient energy generation. We propose that elamipretide will improve cardiac mitochondrial energy metabolism and preserve cardiac performance, ultimately improving survival in sepsis.

METHODS/RESULTS
We aim to characterize myocardial depression and cardiac mitochondrial dysfunction in sepsis, and evaluate the therapeutic efficacy of elamipretide in improving cardiac function in sepsis-induced cardiomyopathy. A validated fecal slurry (FS) induced peritonitis (FIP) mouse model of sepsis was utilized whereby mice were injected intraperitoneally with fecal slurry (0.55 mg/kg) or dextrose vehicle. Additional intervention groups were included whereby elamipretide (10 mg/kg) or PBS vehicle were administered 1-hour after FS-injection. 12 hours and 10 days post-inoculation, cardiac contractile capacity and ventricular filling ability were evaluated with speckle-tracking echocardiography. Left ventricular (LV) pressure-volume loop acquisition was used to elucidate load-independent cardiac and hemodynamic (mal)adaptations in sepsis. Biochemical assays were conducted to investigate inflammatory infiltration, markers of cardiac and kidney cell stress and injury, and activities of metabolic enzymes.
LV ejection fraction, cardiac output, and stroke volume were diminished in untreated septic mice, but elamipretide treatment significantly improved these parameters. Stroke work, cardiac inotropic capacity, cardiac efficiency, and ventriculo-arterial coupling indices were compromised in sepsis, and were significantly improved with elamipretide intervention.

CONCLUSIONS
Elamipretide is a promising therapeutic candidate for the prevention of immediate and long-standing sepsis-induced cardiovascular decline by restoring myocardial ATP production and improving systolic and diastolic cardiac performance.

Session 4, 3MT-style presentation

Characterizing the left ventricular transcriptome of donation after circulatory death (DCD) porcine hearts undergoing prolonged ex situ heart perfusion (ESHP) in the absence and presence of a multi-drug postconditioning treatment

Fulin Wang, Phing-How Lou, Eliana Lucchinetti, Darren H. Freed, Michael Zaugg

BACKGROUND
We have previously shown that a multi-drug postconditioning treatment of Intralipid, sevoflurane and remifentanil improved the function and viability of extended criteria donation after circulatory death (DCD) porcine hearts undergoing prolonged ex situ heart perfusion (ESHP). However, the changes in the cardiac tissue transcriptome as a result of the prolonged ESHP and multi-drug postconditioning treatment have not been investigated.

METHODS/RESULTS
Porcine DCD hearts were mounted on a custom ESHP apparatus and perfused with or without the multi-drug postconditioning treatment for 6 hours (n=5 per group). The multi-drug postconditioning treatment consisted of 1% Intralipid, 2% (v/v) sevoflurane and 3 nM remifentanil given at the onset of ESHP. Hearts not subjected to the ESHP process served as an unperfused, native control (n=8). Left ventricular tissue from a total of 18 hearts were collected and processed for next generation RNA sequencing. Data was analyzed using SEQUIN (https://sequin.ncats.io/app/) and Gene Set Enrichment Analysis software.
Of the 21,849 genes identified, 5,374 genes were differentially expressed between perfused and unperfused hearts. The postconditioning treatment resulted in 48 differentially regulated genes in perfused DCD hearts. Transcripts involved in mitochondrial metabolism, including components of the electron transport chain and Krebs cycle, were downregulated in perfused hearts. mRNA levels of mitochondrial aminoacyl-tRNA synthetases, a crucial component of mitochondrial protein synthesis, were also reduced in perfused hearts, which restricts the cell's ability to synthesize new proteins particularly when there is cellular stress and protein damage, such as the DCD process and prolonged perfusion. In perfused DCD hearts without postconditioning, transcripts involved in lipid accumulation were upregulated, likely contributing to dysfunctional lipid metabolism and the observed triglyceride accumulation in the tissue. Conversely, transcripts involved in lipolysis and beta-oxidation pathways were enriched in perfused DCD hearts with postconditioning, which were able to effectively use Intralipid as a fuel source and retain their metabolic flexibility. While inflammatory genes, including targets of NFκB, were similarly enriched in perfused hearts, only perfused DCD hearts without postconditioning developed a mRNA signature typically observed in cardiomyopathies.

CONCLUSIONS
DCD hearts undergoing prolonged ESHP have reduced transcript levels of proteins involved in mitochondrial protein synthesis and metabolism, in addition to upregulation of genes involved in inflammation and cardiac remodeling. However, the multi-drug postconditioning treatment attenuated the impairment and dysfunction of mitochondrial metabolism, and prevented maladaptive remodeling and development of a cardiomyopathy-like mRNA signature in DCD hearts.

Poster #23

Mapping endothelial genetic signature alterations and vascular structural changes in the human decidua across the first trimester

Wilson, Bethan & Riddell, Meghan

BACKGROUND
Adaptation of decidua basalis vascular structures is required for adequate placental development and critical for pregnancy health. However, mapping of human decidual vascular adaptations aside from spiral artery remodeling is limited. Endothelial cells (EC) are key drivers of angiogenesis and remodeling of vascular networks. Therefore, we mapped EC adaptations in the human decidua basalis across the first trimester of pregnancy using single-cell RNA sequencing (scRNA-seq) and visualised large-scale vascular network remodeling using light sheet microscopy.

METHODS/RESULTS
Methods: ScRNA-seq was performed using 10X genomics on dissociated human decidua basalis, gestational age (GA) 4-13 weeks (n=16). Preprocessing was performed in R (Seurat) and gene ontology (GO) pathway analysis with [g:Profiler]. Decidual tissue sections (1cm3) were stained with anti-CD31 (EC) and anti-cytokeratin-7 (trophoblasts), cleared via an adapted iDISCO protocol, imaged by light sheet microscopy, and quantified with Imaris software.

Results: Top EC differentially expressed genes (DEG) included higher expression of ANGPT2, important for vascular regression and leakage, and the key EC transcription factor ETS2 in <10wk GA versus > 10wk GA EC. GO pathway analysis revealed enrichment of EC gene expression associated with cell motility at <10wk GA, suggesting structural adaptations through EC migration in the early first trimester. Imaging analyses revealed a shift towards large caliber vessels from early to late first trimester, with evidence of vascular fusion at 7.5wks GA to facilitate rapid enlargement of vessels without proliferation.

CONCLUSIONS
Our results reveal that the human decidual vasculature develops high calibre blood vessels in the near absence of EC proliferative gene signatures. The sum of our data indicate migratory vascular remodeling dominates the early-first trimester, and vascular fusion between adjacent vessels may rapidly facilitate an ~4-fold increase in decidual blood flow. Therefore, disruption of EC migration or vascular fusion could limit vascular capacitance and contribute to the development of placental pathologies.

Session 2, Vascular Function oral presentation

Progression of Atherosclerotic Cardiovascular Disease in Young Women with and without Polycystic Ovary Syndrome

Xiaoying Wu, Jesse Batara, Mahua Ghosh, Paolo Raggi, Harald Becher, Donna Vine

BACKGROUND
Polycystic Ovary Syndrome (PCOS) is the most prevalent endocrine-metabolic disorder, affecting approximately 10-15% of women across the lifespan. Women with PCOS are at increased risk of obesity, diabetes and cardiovascular disease (CVD). We have previously shown high-risk overweight-obese women with and without PCOS exhibit atherogenic dyslipidemia, with elevated TG, apoB and remnant-cholesterol, and left ventricular (LV) hypertrophy and diastolic dysfunction (E/A ratio, IVRT), compared to healthy-weight controls. Those with PCOS have increased atherosclerotic cardiovascular disease (ACVD) with a 35%-56% higher carotid plaque height (CPH) compared to controls, and a 14% higher carotid intimal medial thickness (cIMT), compared to healthy-weight controls. There is limited data on early ACVD and cardiac dysfunction and progression of these indices in young women with and without PCOS. The aim of this study was to examine progression of atherogenic dyslipidemia, cardiac dysfunction and ACVD in a cohort of young women with and without PCOS at baseline and at 2 years follow up.

METHODS/RESULTS
A cohort of overweight-obese (BMI >25kg/m2) females aged 18-45 years with and without PCOS matched for age-BMI, and healthy-weight controls were assessed at baseline and at 2 years follow up. Measurements included blood lipids and apoB, remnant-cholesterol, hormones, insulin-glucose, ACVD (CPH, cIMT) and cardiac function using 2D and 3D-echocardiography.

To date, 15 PCOS, 5 non-PCOS controls and 3 healthy-weight controls have completed follow up testing, with a mean follow-up duration 2.6 years. Our preliminary data shows lipid and hormone profile and cardiac function had similar trends to baseline data across groups. cIMT increased from baseline by 11.8% in PCOS, compared to 1.57% in non-PCOS and 8.24% in healthy-weight controls. The progression of cIMT/yr was 0.8-1.4% higher in PCOS (3.57±1.26) compared to non-PCOS (2.14±0.42) and healthy-weight controls (2.82±0.73). Of those who had carotid plaque at baseline, CPH increased 6-15 fold in those with PCOS compared to controls at follow-up.

CONCLUSIONS
Our preliminary follow-up data shows that high-risk young women with PCOS have exacerbated CVD risk factors and accelerated progression of atherosclerotic CVD compared to age-BMI matched and healthy-weight controls. Therefore, early screening and detection, and targeted interventions to mitigate CVD development in high-risk women with and without PCOS may be warranted in CVD prevention guidelines for women.

Figure 1. Fasting Plasma Lipids, Carotid Intima-Media Thickness and Plaque Height in Healthy-weight Controls, Non-PCOS and PCOS at Baseline and Follow-Up.

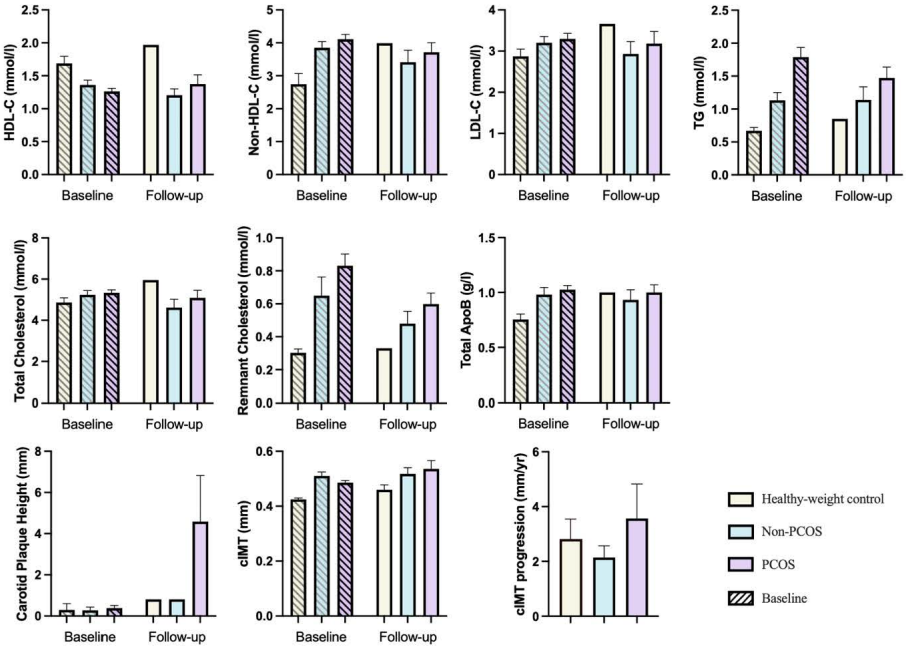

Table 1. Participant Characteristics in Healthy-weight Controls, Non-PCOS and PCOS at Baseline and Follow-Up.

	HWC (Baseline) n=3	Non-PCOS (Baseline) n=5	PCOS (Baseline) n=15	HWC (follow-up) n=3	Non-POCS (Follow-up) n=5	PCOS (Follow-up) n=15
Age (y)	31.67±3.53	30.20±1.77	34.33±1.42	34.33±3.28	32.80±1.93	37.29±1.21
BMI (kg/m^2)	20.62±0.16	37.62±4.28	39.15±2.32	22.42±1.42	41.41±3.06	37.66±5.50
Follow-up Duration (y)				2.78	2.70	2.56
Fat (%)	24.97±3.03	41.96±4.17	47.41±2.10	28.80±2.47	48.63±3.07	47.04±2.02
Fat Free Mass (%)	72.10±1.30	58.04±4.17	52.59±2.10	71.20±2.47	51.38±3.07	52.96±2.02
Glucose (mmol/l)	4.77±0.14	5.21±.16	5.02±0.08	4.40±0.00	4.81±0.10	5.35±0.26
Insulin (pmol/l)	55.50±2.50	90.33±12.41	160.7±29.2	22.00±0.00	152.1±31.97	121.7±15.79
HOMA-IR	1.95±0.05	3.17±0.52	6.93±1.22	0.70±0.00	5.40±1.12	4.96±0.74
Total Testosterone (nmol/l)	0.90±0.10	0.83±0.20	0.93±0.17	1.4±0.00	1.15±0.87	1.05±0.13
Free Testosterone (pmol/l)	11.00±1.00	14.15±4.55	14.09±3.86	17.20±0.00	25.25±2.69	21.63±3.88
SHBG (nmol/l)	60.00±18.00	31.00±3.27	33.01±7.87	59.00±0.00	24.25±1.38	35.67±5.37
Free Androgen Index	1.59±0.31	2.93±1.00	11.21±7.46	2.37±0.00	4.85±-0.63	4.10±1.00

Values are expressed as mean±SEM. Abbreviation: BMI, body mass index; HOMA-IR, homeostatic model assessment for insulin resistance; SHBG, sex hormone biding globulin.

Poster #24

Cardioprotective Response and Senescence in Aged sEH Null Female Mice Exposed to LPS

Ala Yousef, Deanna K. Sosnowski, Liye Fang, Renald James Legaspi, Jacob Korodimas, Andy Lee, Katharine E. Magor, John M. Seubert

BACKGROUND
Deterioration of physiological systems, like the cardiovascular system, occurs progressively with age impacting an individual's health and increasing susceptibility to injury and diseases. Cellular senescence has an underlying role in age-related alterations and can be triggered by natural aging or prematurely by stressors such as the bacterial toxin, lipopolysaccharide (LPS). The metabolism of polyunsaturated fatty acids (PUFAs) by CYP450 enzymes produces numerous bioactive lipid mediators that can be further metabolized by soluble epoxide hydrolase (sEH) into diol metabolites, often with reduced biological effects.

METHODS/RESULTS
Methods: Young (2-5 months) and aged (18-25 months) female wild type (WT), and sEH null mice were administered either saline (control), or 10 mg/kg LPS via i.p. injection. Echocardiography was used to assess cardiac function at baseline and 24 hours after injections. Results: Age-related cardiac differences in female mice was observed, where young mice demonstrated resistance to LPS injury, and genetic deletion or pharmacological inhibition of sEH attenuated LPS-induced cardiac dysfunction in aged female mice. Bulk RNA-sequencing analyses revealed transcriptomics differences in aged female hearts. Confirmatory analysis demonstrated changes to inflammatory and senescence gene markers such as Il-6, Mcp1, Il-1β, Nlrp3, p21, p16, and SA-β-gal were attenuated in the hearts of aged female mice where sEH was deleted.

CONCLUSIONS
Collectively, these findings highlight the role of sEH in modulating the aging process of the heart, whereby targeting sEH is cardioprotective.

Graphical Abstract

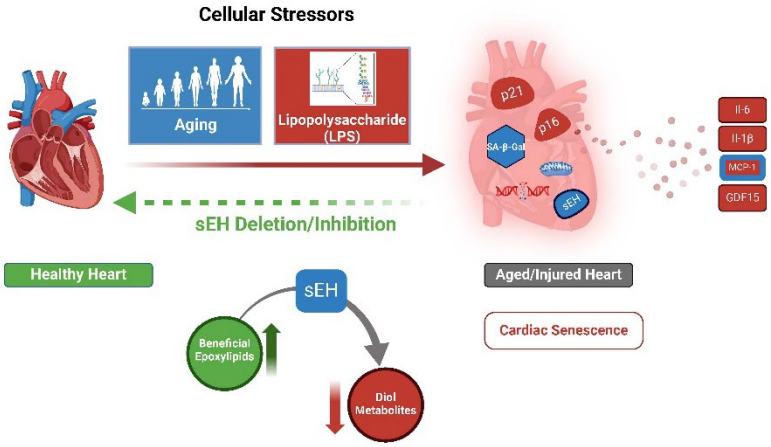

Poster #25

Unveiling Geographic Patterns in Critical Congenital Heart Defects: A Spatial Analysis of Selected airPollutants

Ghazal Zargari, Payam Amini, Asim Thapa, Ari Joffe, Charlene Robertson, Irina Dinu

BACKGROUND
Critical congenital heart defects (cCHD) present significant health challenges, often leading to surgical intervention or infant mortality within the first month of life. While chromosomal abnormalities contribute to cCHD, recent research highlights the role of environmental factors, including air pollution.

METHODS/RESULTS
In this study, we employed geographically weighted multinomial logistic regression (GWMLR) to investigate the intricate relationship between exposure to four air pollutants (PM2.5, ozone, NO2, and AQSMK) and critical congenital heart defects (cCHDs) subtypes, aiming to unveil spatial variations. Analysis of 1,484 infants revealed significant associations between PM2.5 and cCHDs in 0.18% of the locations, and ozone in 7.13% of the locations. Disparities were noted in the subtypes linked to these pollutants compared to the original dataset, highlighting nuanced spatial patterns. Clustered significant locations indicate localized impacts of environmental stressors such as industrial activities. Despite significance, odds ratios consistently fell below 1, possibly due to selecting known chromosomal cCHDs as the reference group, implying potential baseline risk underestimation and thus urging caution in interpretation.

CONCLUSIONS
This study emphasizes the complex interplay of genetic predispositions and pollutant exposures. Significance in small clusters underscores varied spatial influences of pollutants on cCHD incidence, necessitating targeted interventions.

Session 4, 3MT-style presentation

A critical contribution of cardiac myofibroblasts and a predictive role of UCP2 SNPs in the RV decompensation in pulmonary hypertension

Yongneng Zhang, Alois Haromy, Yongsheng Liu, Yuanyuan Zhao, Gopinath Sutendra, Evangelos D. Michelakis

BACKGROUND
The mechanism driving the transition from compensated (cRVH) to decompensated right ventricular hypertrophy (dRVH) in pulmonary hypertension (PHT) is unknown. We hypothesized that a transition from cardiac fibroblasts (cFB) to cardiac myofibroblasts (cMFB) underlies this mechanism. Decreased mitochondrial calcium (mCa++) promotes cMFB differentiation (from cFB). Methylation of mCa++ uptake 1 (MICU1) and lack of UCP2 (uncoupling protein 2, a component of the mCa++ uniporter complex) decrease mCa++.

METHODS/RESULTS
Methods: In a monocrotaline-rat PHT model, we separated cRVH from dRVH based on strict hemodynamics and Echo. We measured the RV pressure from isolated perfused hearts and sarcomere shortening from isolated RV cardiomyocytes. In a cohort (n=72) of patients with PHT, the correlation between UCP2 loss-of-function SNP (rs659366) and RV function was measured.

Results: In isolated hearts, RV systolic pressure was lower in dRVH but in isolated cardiomyocytes (CM), contractility (sarcomere shortening) was not, pointing to a non-cardiomyocyte difference. The number of cMFB was dramatically increased in dRVH compared to Control and cRVH. Mitochondrial respiration was lower in dRVH cMFB than cRVH cFB. mCa++ was progressively decreased from Control to cRVH to dRVH c(M)FB, while it was not different in CM. The MICU1 methyltransferase (PRMT1) levels and MICU1 methylation were increased but the expression of UCP2 was decreased from Control to cRVH to dRVH c(M)FB (but not CM). In human RV tissues (from autopsy or biopsy, n=60), dRVH had increased number of cMFB compared to Control and cRVH. Cytoplasmic PRMT1 was increased and UCP2 was decreased from Control to cRVH to dRVH c(M)FB. In patient cohorts, carriers of the loss-of-function UCP2 SNP had decreased TAPSE compared to non-carriers that had similar mean PA pressure.

CONCLUSIONS
A change of cell identity (cFB to cMFB) in the RV may be the basis of cRVH to dRVH transition, rather than contractile failure of CM. UCP2 SNP may predict early dRVH, if confirmed in larger cohorts.

Poster #26

The relationship of diuretics and dietary sodium in patients with heart failure: an analysis of the SODIUM-HF trial

Kevin Zhou, Wendimagegn Alemayehu, Sarah Rathwell, and Justin A. Ezekowitz

BACKGROUND
SODIUM-HF was a large clinical trial testing dietary sodium restriction compared to usual care in patients with heart failure that showed no reduction in the rate of the primary endpoint of clinical events. It has been suggested that diuretic doses in response to dietary sodium modification may have influenced the trial results.

Objective: We assessed the effects of baseline diuretic dose and diuretic dose changes on clinical outcomes in the SODIUM-HF trial.

METHODS/RESULTS
Methods: Diuretics were converted to furosemide-equivalent diuretic total daily doses. Furosemide dose ranges were treated as continuous variables and also stratified into 0 mg, 1–39 mg, 40 mg, 41–80 mg, and >80 mg. The baseline diuretic dose and change in diuretic dose were assessed and correlated with dietary sodium restriction and changes in dietary sodium intake. Finally, we examined the relationship between diuretic dosing and primary outcome of SODIUM-HF (cardiovascular-related ED visit, cardiovascular-related hospitalization, and all-cause mortality).

Results: Of the 806 patients enrolled in the SODIUM-HF trial, 784 had known diuretic status categorized as follows: 209 patients (26.7%) with 0 mg, 134 patients (17%) with 1-39 mg, 205 patients (26.1%) with 40 mg, 118 patients (15.1%) with 41-80mg, and 118 patients (15.1%) >80 mg. No correlation was found between dietary sodium intake and diuretic dose either at baseline or throughout the trial. For patients on >0 mg of baseline diuretic dose, the relative 2-year risk of clinical outcomes was higher compared to the 0 mg patient cohort (Figure 1a, $p<0.05$). No association was demonstrated between the outcomes and change in diuretic dose at 6 months. There was no significant difference in the treatment effect of dietary sodium restriction on outcomes between baseline diuretic dose levels (Figure 1b, all interaction $p>0.05$).

CONCLUSIONS
A higher baseline diuretic dose in patients in SODIUM-HF was associated with worse clinical outcomes. Baseline and change in diuretic dose or dietary sodium were not associated with a difference in primary outcomes when comparing usual care and dietary sodium restriction.

Figure 1a. Relative risk of 2-years outcomes according to diuretic dose at *baseline*. Adjusted HRs represent the risk compared to that of patients with no diuretic use (0 mg).

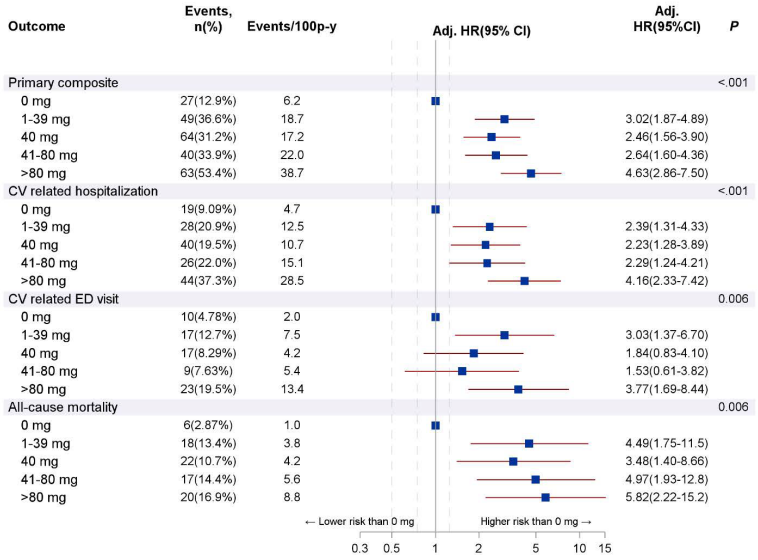

Figure 1b. Low sodium treatment effect by diuretic dose level at *baseline*.

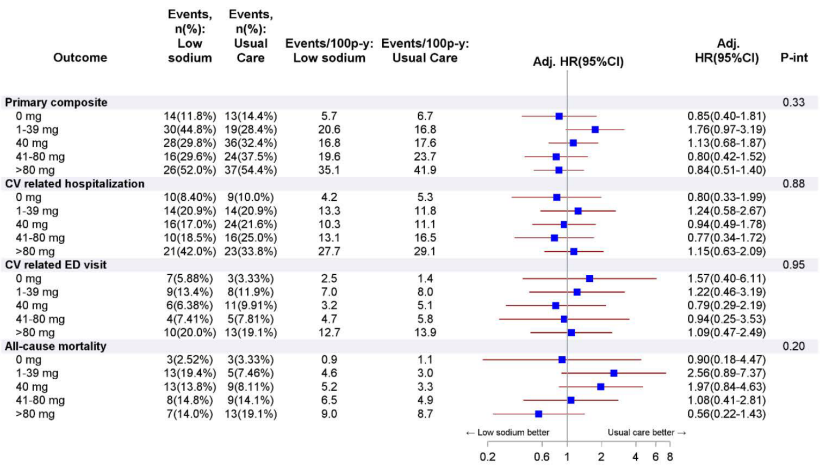

Session 3, Cardiac Function oral presentation

Improved mitochondrial respiration in a murine model of heart failure through the modulation of ROMO1

Matthieu Zolondek, Matthew Martens, Heidi L. Silver, Mostafa Khairy, Daniela Morales-Lamas, Mourad Ferdaoussi, Helene Lemieux, Jason R.B. Dyck

BACKGROUND
Heart failure (HF) is essentially a disease where poor heart function limits the supply of blood to meet the metabolic demands of the body. Changes in the functional capacity of the failing heart are often made worse as a result of defective cardiomyocyte mitochondria. Recently, we demonstrated the role of a small mitochondrial protein named reactive oxygen species modulator 1 (ROMO1) as a regulator of cardiomyocyte mitochondrial respiration in both the healthy and the failing heart. We also observed improved heart function in mice with HF following gene-therapy based cardiomyocyte-specific ROMO1 overexpression. Based on this, we hypothesized that the observed increase in cardiac function was due to ROMO1 improving mitochondrial respiration through the electron transport system.

METHODS/RESULTS
We sought to explore the effect of ROMO1 overexpression on cardiac metabolism in heart failure. To do this, we overexpressed ROMO1 in a cardiomyocyte-specific manner using adenoviral associated gene delivery of ROMO1 (AAV9-αMHC-ROMO1) or control (AAV9-aMHC-Null) expressing viruses, and subjected male mice (n = 24) to sham control surgeries or HF-inducing transverse aortic constriction (TAC) surgery. Cardiac function was evaluated 2.5 weeks post-surgery using transthoracic echocardiography. We observed a significant decrease in cardiac function following TAC that was significantly reduced by ROMO1 overexpression. Cardiac mitochondrial respiratory capacity from these hearts was evaluated using High-Resolution Respirometry (Oroboros Instruments; Innsbruck, Austria). Hearts from AAV-control TAC mice demonstrated a significant reduction in maximal respiration (spare respiratory capacity (SRC); SEM=0.039, p=0.0002), and relative oxygen flux through complex I (SEM=0.0855, p=0.01) and complex II (SEM=0.038, p=0.0002) of the respiratory system. Hearts from AAV-ROMO1 TAC mice resulted in a significant recovery in all three measures, demonstrating total normalization of mitochondrial function (SRC, SEM=0.023, p=0.02; CI, SEM=0.066, p=0.008; CII, SEM=0.037, p=0.02). Importantly, SRC was found to be significantly correlated with ejection fraction (p=0.0004), demonstrating the intimate relationship between ROMO1-mediated cardiac metabolism and heart function.

CONCLUSIONS
Our preliminary study characterized the mitochondrial metabolic state in the hearts of mice subjected to HF and observed decreases in mitochondrial oxidative capacity and respiratory chain function. Additionally, overexpression of ROMO1 using our gene therapy-based approach in the heart was sufficient to prevent loss of mitochondrial oxidative capacity following TAC. This restoration of mitochondrial function occurred alongside a restoration of cardiac function, demonstrating the importance of normal mitochondrial function in HF development.

Thank you for joining us!!